

This is the peer reviewed version of the following article:

A mechanical model for thin sheet straight cutting in the presence of an elastic support / Shugailo, T.; Nobili, A.; Mishuris, G.. - In: INTERNATIONAL JOURNAL OF ENGINEERING SCIENCE. - ISSN 0020-7225. - 193:(2023), pp. 103964-103964. [10.1016/j.ijengsci.2023.103964]

Terms of use:

The terms and conditions for the reuse of this version of the manuscript are specified in the publishing policy. For all terms of use and more information see the publisher's website.

27/09/2024 02:17

(Article begins on next page)

International Journal of Engineering Science

A mechanical model for thin sheet straight cutting in the presence of an elastic support

--Manuscript Draft--

| | |
|------------------------------|---|
| Manuscript Number: | |
| Article Type: | Full Length Article |
| Section/Category: | Solids and Materials |
| Keywords: | Linear Fracture Mechanics; Foundation; Stress Intensity Factors; Thin sheet cutting |
| Corresponding Author: | Andrea Nobili, Ph.D. Università degli Studi di Modena e Reggio Emilia: Università degli Studi di Modena e Reggio Emilia Modena, ITALY |
| First Author: | Timofei Shugailo |
| Order of Authors: | Timofei Shugailo Andrea Nobili, Ph.D. Gennady Mishuris, PhD |
| Abstract: | <p>We study the mechanics of sheet straight cutting in terms of a linear elastic fracture mechanics (LEFM) problem for a infinite thin elastic Kirchhoff plate partly supported by a Winkler foundation. The plate features a semi-infinite crack that is located at the edge of the supported zone and that is subjected to shear and bending loads, representing the action of the cutting tool (e.g. scissors blades). The fact that the plate is only partly supported by the foundation significantly complicates the analysis for it creates a non-symmetric framework, both locally and globally. Yet, a semi-analytical solution is obtained through casting the matrix Wiener-Hopf problem in terms of a pair of convolution integral equations defined on a semi-infinite domain. Stress intensity factors (SIFs) are obtained which converge to the known limits for a symmetric and skewsymmetric free plate. This analysis reveals the fundamental role played by the support in affecting the SIFs in an opposing manner, by enhancing/decreasing the symmetric/skew-symmetric components. Consequently, changing the support stiffness is capable of shifting the failure mechanism, from bending to shear. This observation may be taken advantage of when cutting materials which are more sensitive to either of these failure mechanisms. Also, it proves that the role of the support cannot be neglected when developing mechanical models of any cutting process.</p> |
| Suggested Reviewers: | Giuseppe Saccomandi, PhD Full Professor, University of Perugia giuseppe.saccomandi@unipg.it Established expert in the field of solid mechanics |
| | Micheal Nieves, PhD Senior Lecturer, Keele University m.nieves@keele.ac.uk Expert in the field of fracture mechanics |
| | Victor Eremeev University of Cagliari victor.eremeev@unica.it Expert in the field of material fracture |



UNIMORE

UNIVERSITÀ DEGLI STUDI DI
MODENA E REGGIO EMILIA

August 10th, 2023

Dear Editor,

Please find enclosed, the research paper

“A mechanical model for thin sheet straight cutting in the presence of an elastic support”

by

T. Shugailo, A. Nobili and G. Mishuris

submitted for consideration in the International Journal of Engineering Science.

The paper presents a new solution in LEFM for a crack thin plate partly supported by an elastic foundation.

To the best of the authors' knowledge, it is the first contribution that investigates the role of the (partial) support in affecting the cutting process, especially in terms of the stress intensity factor and of the corresponding failure mode of the material.

The material is original and it has not been submitted for publications in other journals.

The authors are aware of the ethical guidelines put forward by the journal and fully adhere to it.

The authors are in no conflict of interest regarding the material presented in this paper.

This version of the paper is approved by all authors.

Best regards,

Andrea Nobili

(Corresponding author)

Highlights of the paper

A mechanical model for thin sheet straight cutting in the presence of an elastic support

- We consider the role of partial elastic support in the problem of a semi-infinite linear crack located at the edge of the supported zone for a thin elastic plate
- We find that the support acts as coupling between the bending and the shearing stress intensity factors (SIFs)
- Consequently, the material failure mode is fundamentally driven by the stiffness of the support which cannot be ignored in any modelling of cutting
- The support stiffness affects the SIFs in opposing fashion, decreasing one and increasing the other
- It also determines the asymptotics of the solution in the far-field for the unsupported plate
- The limiting situation of infinite support stiffness corresponds to a free cracked plate under symmetric/skew-symmetric conditions, depending on the loading
- In no case it corresponds to a cracked plate with built-in semi-edge.

A mechanical model for thin sheet straight cutting in the presence of an elastic support

Timofei Shugailo^b, Andrea Nobili^{a,*}, Gennady Mishuris^b

^a*Dipartimento di Ingegneria Enzo Ferrari, via Vivarelli 10, 41125 Modena, Italy*

^b*Institute of Mathematical and Physical Sciences, Aberystwyth University, Ceredigion SY23 3BZ, Wales, UK.*

A mechanical model for thin sheet straight cutting in the presence of an elastic support

Timofei Shugailo^b, Andrea Nobili^{a,*}, Gennady Mishuris^b

^a*Dipartimento di Ingegneria Enzo Ferrari, via Vivarelli 10, 41125 Modena, Italy*

^b*Institute of Mathematical and Physical Sciences, Aberystwyth University, Ceredigion SY23 3BZ, Wales, UK.*

Abstract

We study the mechanics of sheet straight cutting in terms of a linear elastic fracture mechanics (LEFM) problem for a infinite thin elastic Kirchhoff plate partly supported by a Winkler foundation. The plate features a semi-infinite crack that is located at the edge of the supported zone and that is subjected to shear and bending loads, representing the action of the cutting tool (e.g. scissors blades). The fact that the plate is only partly supported by the foundation significantly complicates the analysis for it creates a non-symmetric framework, both locally and globally. Yet, a semi-analytical solution is obtained through casting the matrix Wiener-Hopf problem in terms of a pair of convolution integral equations defined on a semi-infinite domain. Stress intensity factors (SIFs) are obtained which converge to the known limits for a symmetric and skew-symmetric free plate. This analysis reveals the fundamental role played by the support in affecting the SIFs in an opposing manner, by enhancing/decreasing the symmetric/skew-symmetric components. Consequently, changing the support stiffness is capable of shifting the failure mechanism, from bending to shear. This observation may be taken advantage of when cutting materials which are more sensitive to either of these failure mechanisms. Also, it proves that the role of the support cannot be neglected when developing mechanical models of any cutting process.

Keywords: Linear Fracture Mechanics; Foundation; Stress Intensity Factors; Thin sheet cutting

1. Introduction

In a typical sheet cutting process, a sheet of material is divided in two parts through application of a pair of large enough forces as to cause material failure. A common example is metal sheet cutting, which usually occurs by applying a shearing force, for example through a punch, to the sheet resting on a die (in which case the process is named "punching"). This process is sometimes referred to as shearing cutting (Figure 1) and it belongs to the large family of manufacturing procedures aimed at deforming a metal, such as blanking (making holes in a sheet), bending, calendaring and slitting. The same basic process occurs when tearing paper with a ruler or along a table edge, as in Figure 2, for the edge operates as the cutting tool and, most importantly, the paper has to be carefully kept well in place (like from a die) for the operation to take place smoothly.

Alternatively, a pair of blades may be used, as in familiar scissor cutting. The cutting process is generally delicate and error prone, in dependence of material flaws but also of imperfections in applying the right constraining conditions, which prove crucial [2]. In particular, it is easy to see that, at the microscale, crack formation and propagation induced by the cutting process proceed in zig-zag fashion, although this may not appear so clearly at the macroscale. However, this feature may sometimes also emerge at the macroscale, when the material crack unexpectedly deviates from the straight path. In fact, we show that this behaviour is not extraneous to the classical theory of cracks, which is traditionally based on linear elastic fracture mechanics (LEFM) results that are crucially supplemented by a local symmetry requirement to predict the crack path [14, 7]. This is well straightforward inasmuch as the geometry under consideration indeed supports such symmetry requirement, at least locally, and this is in fact the case of many fracture mechanics problems

*Corresponding author

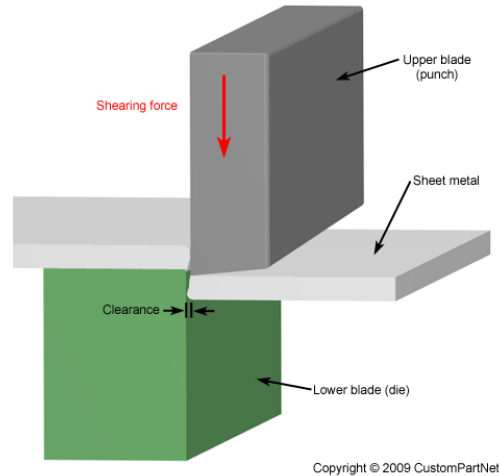


Figure 1: Schematics of shearing cutting of a steel sheet

21 which may be solved explicitly [1, 27, 17, 19]. Remarkably, they form the basis of many technical solutions
 22 that are applied, in the form of guidelines or codes, for the design of thin light structures, especially in the
 23 shape of shells and plates for the aerospace and high performance sectors [27, 13, 6]. The matter becomes
 24 blurred when general non-symmetric conditions are dealt with, precisely in the close neighborhood of the
 25 crack tip.

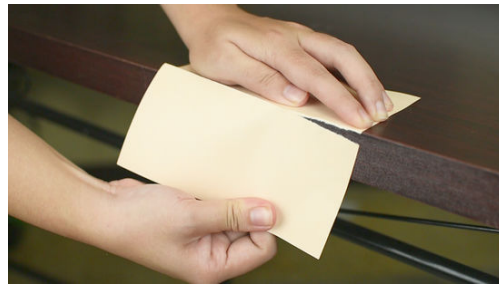


Figure 2: Tearing paper along a table edge

26 Clearly, the problem of cutting, even in the case of brittle materials, cannot be fully represented within
 27 the framework of LEFM, given that elasto-plastic, nonlinear, thermo-mechanical and irreversible processes
 28 may play an important role [2]. Consequently, for the full picture, numerical methods have to be reverted to
 29 in order to solve the nonlinear coupled model which emerges. However, even then, the starting point is often
 30 the stress intensity factor (SIF) of LEFM, to avoid attacking an overwhelmingly complicated problem, see,
 31 for example, [4] and [33, Chap.6]. Moreover, it is most striking that, to our best knowledge, no contributions
 32 are available in the literature which take into consideration the role of the support (the die) in affecting
 33 the mechanics of the cutting. This is all the more remarkable if one considers that any cutting, say scissor
 34 cutting, cannot take place without the action of a support, if only in consideration of the fact that cutting
 35 forces can never be fully self-equilibrated (whence the role of the clearance in Fig.1). Further, we mention
 36 that other pathways to failure exist beside cracking, as described in [32] for delamination.

37 Only a limited number of crack problems have been solved analytically within elastic plate theory [29],
 38 and this despite the utmost practical importance of these structures in engineering applications [15, Chap.11].
 39 The reasons behind this shortcoming may be traced to the difficulties attached to solving a fourth order PDE
 40 with complicated boundary conditions, for which the superposition principle is of limited help. Consequently,
 41 only symmetric or skew-symmetric conditions could be solved in general [28]. When introducing an elastic
 42 foundation, matters become even more intricate, because, from a mathematical standpoint, the presence of
 43 the foundation destroys the homogeneous character of the plate PDE. In their pioneering work, [1] could

44 work out the SIFs in bending of a fully supported plate, that is a symmetric setting. This work was later
 45 extended to a weakly nonlocal foundation [17, 18] and then generalized to dynamical effects [19]. Incidentally,
 46 these problems are also very relevant to the engineering design of pavements [25]. The case of a finite crack
 47 and of a shell were considered by [5] and later by [16], while a simplified 3D theory was adopted in [9].
 48 In [3], a closed-form Green function for a Griffith crack or a rigid line inclusion (anticrack) in an infinite
 49 anisotropic elastic plate could be obtained. These results were recently improved by [10] to reconcile the rigid
 50 body motions of the plate with that of the inclusion. The problem of studying the role of the foundation in
 51 affecting crack propagation is conceptually similar to that recently considered in [24], where crack penetration
 52 is antagonized by contrast in fracture toughness. In such studies, analysis of the Energy Release Rate (ERR)
 53 or, equivalently, of the SIF, plays a crucial role [23]. Moreover, specific boundary conditions may significantly
 54 influence not only the those fracture measures, but even leads to different singularities at the crack/defect
 55 tip. For example, if one considers surface stress prescribed along the body surface, the relations between the
 56 ERR and SIFs may change, as well as the stress singularity itself [8] that requires an additional separate
 57 analysis in terms of possible fracture initiation/propagation.

58 In this paper, we investigate the fundamental LEFM problem of an infinite thin elastic Kirchhoff plate
 59 partially supported by an elastic local (Winkler) foundation (the die). The plate sustains a semi-infinite
 60 rectilinear crack, located precisely along the foundation edge, which is loaded, in continuous fashion, at the
 61 crack flanks, to simulate the cutting tool action, for example the scissors blades. Spotlight is set on determin-
 62 ing the stress intensity factors and, in particular, on being able to assess the role of the foundation properties
 63 on the cutting process and specifically on its path. The problem is laid out in Section 2 and then recast in
 64 the Fourier domain in Sec.3 in the form of a pair of inhomogeneous Weiner-Hopf functional equations [21].
 65 Since the kernel matrix is non-diagonal, this coupled problem cannot be tackled in general. This difficulty
 66 is overcome first by regularization (Sec.4) and subsequently by reduction to a pair of Fredholm convolution
 67 equations (Sec.5), which are then solved numerically (Sec.6). In an attempt to lighten the mathematical
 68 structure of the manuscript, detailed derivations have been moved to the Appendix. Conclusions are drawn
 69 in Sec.7. Results compare favourably with the limiting cases of a free plate under symmetric and skew-
 70 symmetric global conditions (see Sec.Appendix A). Interestingly, the limiting case of an exceedingly stiff
 71 (weak) support does not correspond to the solution of a built-in (free) half-plate, unless special symmetries
 72 are assumed for the loading.

73 2. Governing equations

74 Let us consider an infinite Kirchhoff plate partially supported by a Winkler elastic foundation and par-
 75 tially free (Fig.3). A Cartesian reference frame is attached to the plate in such a manner that the x -axis
 76 coincides with the transition line at the supported/free zone. We assume that the supported plate occupies
 77 the upper half-plane A, $y > 0$, and the free plate is located in the lower half-plane B, $y < 0$. A semi-infinite
 rectilinear crack is located at negative values of the x -axis. The governing equation for the transverse

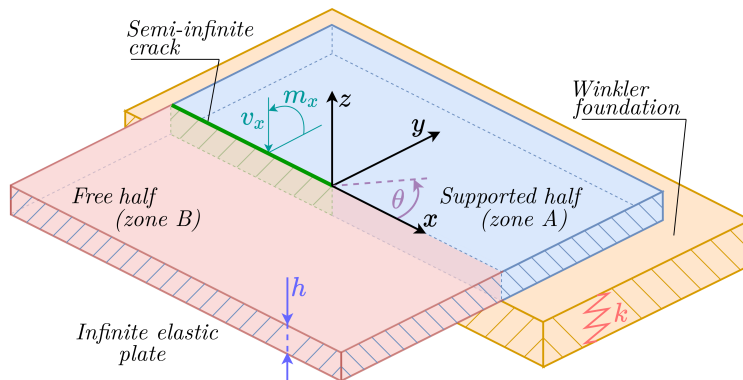


Figure 3: A Kirchhoff plate partially supported on a Winkler elastic foundation

78 displacement of the plate u_z reads
 79

$$D\Delta\Delta u_z = q - \pi, \quad (1)$$

80 being $\Delta = \partial_{xx} + \partial_{yy}$ the Laplace operator in two dimensions, q the transverse distributed load, $D =$
 81 $Eh^3/(12(1 - \nu))$ the plate bending stiffness and π the soil reaction. Here, E is Young modulus and ν
 82 Poisson's ratio. For the case at hand, the soil reaction is given by

$$\pi = \begin{cases} ku_z, & y > 0, \\ 0, & y < 0, \end{cases} \quad (2)$$

83 wherein k is Winkler elastic modulus. Assuming no applied external loading, Eqs.(1, 2) may be rewritten as
 84 (cf.[20] in the static framework)

$$\begin{cases} \Delta\Delta u_z + \lambda^{-4}u_z = 0, & y > 0, \\ \Delta\Delta u_z = 0, & y < 0. \end{cases} \quad (3)$$

85 having let the plate bending length scale

$$\lambda = \sqrt[4]{\frac{D}{k}}.$$

86 Hereinafter, we adopt the dimensionless variables

$$(x_1, x_2, w) = \lambda^{-1}(x, y, u_z). \quad (4)$$

87 Besides, we denote by $w^{A,B}$ the restriction of w to the domain above (below) the crack line, namely
 88 $w^{A,B}(x_1, x_2) = w(x_1, x_2)$ with $x_2 \gtrless 0$. Further, we let the dimensionless quantities: slope (along x_2),
 89 bending moment and Kirchhoff equivalent shearing force (acting across the crack line)

$$\begin{aligned} \phi &= \partial_{x_2} w, \\ m &= (\partial_{x_2 x_2} + \nu \partial_{x_1 x_1}) w, \\ v &= \partial_{x_2} [\partial_{x_2 x_2} + (2 - \nu) \partial_{x_1 x_1}] w, \end{aligned} \quad (5)$$

90 where the last two have been brought in dimensionless form dividing by $D\lambda^{-1}$ and $D\lambda^{-2}$, respectively.

91 The boundary conditions demand continuity beyond the crack-tip

$$\left. \begin{aligned} w^A(x_1, 0) &= w^B(x_1, 0) \\ \phi^A(x_1, 0) &= \phi^B(x_1, 0) \\ m^A(x_1, 0) &= m^B(x_1, 0) \\ v^A(x_1, 0) &= v^B(x_1, 0) \end{aligned} \right\} x_1 > 0, \quad (6)$$

92 and a prescribed continuous (and symmetric) loading at the crack flanks

$$\left. \begin{aligned} m^A(x_1, 0) &= M_0(x_1) \\ m^B(x_1, 0) &= M_0(x_1) \\ v^A(x_1, 0) &= V_0(x_1) \\ v^B(x_1, 0) &= V_0(x_1) \end{aligned} \right\} x_1 < 0, \quad (7)$$

93 where it is understood that $M_0(x_1)$ and $V_0(x_1)$ are the bending moment and shearing force applied at the
 94 crack faces. Symmetry in the applied load is not really important here and it is only assumed for simplicity
 95 because, otherwise, additional balance conditions would be needed.

96 We further assume that the given loads are not singular and decay at infinity:

$$|M_0(x_1)|, |V_0(x_1)| < \infty, \quad x_1 \in (-\infty, 0], \quad (8)$$

97 and

$$M_0(x_1) = O(e^{\gamma_\infty x_1}), \quad V_0(x_1) = O(e^{\gamma_\infty x_1}), \quad x_1 \rightarrow -\infty, \quad (9)$$

98

$$M_0(x_1) = O(|x_1|^{\gamma_0}), \quad V_0(x_1) = O(|x_1|^{\gamma_0-1}), \quad x_1 \rightarrow 0^-, \quad (10)$$

99 where $\gamma_\infty > 0$, $\gamma_0 > 1/2$ are any constants not weaker than the specific behaviour of the solution. Those
100 conditions may be weakened but it is not our goal in this paper.

We agree to add a subscript zero to denote the restriction of a function to the crack line $x_2 = 0$, i.e. $w_0(x_1) = w(x_1, 0)$. Clearly, Eqs.(6) and (7) imply continuity of bending moment and shearing force along the entire x_1 axis. Indeed, taking the difference, we get

$$\llbracket w \rrbracket = 0, \quad \llbracket \phi \rrbracket = 0, \quad x_1 > 0, \quad (11a)$$

$$\llbracket m \rrbracket = 0, \quad \llbracket v \rrbracket = 0, \quad -\infty < x_1 < \infty, \quad (11b)$$

$$m_0^B(x_1) = M_0(x_1), \quad v_0^B(x_1) = V_0(x_1), \quad x_1 < 0. \quad (11c)$$

101 where $\llbracket f \rrbracket = f_0^A - f_0^B$ at $x_2 = 0$.

102 Assuming sufficient decay at infinity, one can observe that the following balance conditions should be
103 satisfied for any $x_2 \leq 0$ (that is in the free plate)

$$\int_{-\infty}^{\infty} v^B(x_1, x_2) dx_1 = 0, \quad \int_{-\infty}^{\infty} m^B(x_1, x_2) dx_1 = 0, \quad \int_{-\infty}^{\infty} x_1 v^B(x_1, x_2) dx_1 = 0, \quad (12)$$

104 expressing vertical and rotational equilibrium about x_1 and x_2 , respectively. In particular, along the sup-
105 ported/free plate transition line $x_2 = 0$, taking into account the conditions (11b), one gets

$$\int_{-\infty}^{\infty} m_0^{A,B}(x_1) dx_1 = 0, \quad \int_{-\infty}^{\infty} v_0^{A,B}(x_1) dx_1 = 0, \quad \int_{-\infty}^{\infty} x_1 v_0^{A,B}(x_1) dx_1 = 0. \quad (13)$$

106 Besides, we anticipate that

$$w(r, \theta) = P_w(x_1, x_2) + r^{3/2} [\mathcal{K}_e w_e(\theta) + \mathcal{K}_o w_o(\theta)] + O(r^2), \quad \text{as } r \rightarrow 0, \quad (14)$$

107 where $\theta \in [-\pi, \pi]$, $\theta = \pm\pi$ corresponding to the upper/lower crack flank, and we have let the rigid body
108 motion (rbm)

$$P_w(x_1, x_2) = \mathcal{W}_0 + \mathcal{W}_1 x_1 + \mathcal{W}_2 x_2.$$

109 Here, we have introduced the polar coordinates (r, θ) such that $(x_1, x_2) = r(\cos \theta, \sin \theta)$. Also, $w_{e,o}(\theta)$ is the
110 even/odd part in θ of the first asymptotic term in the displacement [31, Eq.(8)]

$$w_e(\theta) = -\cos \frac{3\theta}{2} + \frac{3(1-\nu)}{\nu+7} \cos \frac{\theta}{2}, \quad w_o(\theta) = \sin \frac{3\theta}{2} - \frac{3(1-\nu)}{3\nu+5} \sin \frac{\theta}{2}, \quad (15)$$

where $\mathcal{K}_{e,o}$ are the normalized stress intensity factors (SIFs). From the asymptotics (14), we can easily compute the slope, bending moment and shearing force across a surface with normal in the θ direction

$$\phi(r, \theta) = \mathcal{W}_2 + r^{1/2} (\mathcal{K}_e \phi_e(\theta) + \mathcal{K}_o \phi_o(\theta)) + O(r), \quad \text{as } r \rightarrow 0, \quad (16a)$$

$$m_\theta(r, \theta) = r^{-1/2} (\mathcal{K}_e m_e(\theta) + \mathcal{K}_o m_o(\theta)) + \mathcal{M}_0 + O(r^{1/2}), \quad \text{as } r \rightarrow 0, \quad (16b)$$

$$v_\theta(r, \theta) = r^{-3/2} (\mathcal{K}_e v_e(\theta) + \mathcal{K}_o v_o(\theta)) + \mathcal{V}_1 r^{-1} + O(r^{-1/2}), \quad \text{as } r \rightarrow 0, \quad (16c)$$

where

$$\begin{aligned} \phi_e(\theta) &= \frac{3}{2} \left(\cos \frac{3\theta}{2} - \frac{1-\nu}{3\nu+5} \cos \frac{\theta}{2} \right), & \phi_o(\theta) &= \frac{3}{2} \left(\sin \frac{3\theta}{2} - \frac{1-\nu}{\nu+7} \sin \frac{\theta}{2} \right), \\ m_e(\theta) &= \frac{3}{4} (1-\nu) \left(\cos \frac{3\theta}{2} + \frac{3\nu+5}{\nu+7} \cos \frac{\theta}{2} \right), & m_o(\theta) &= -\frac{3}{4} (1-\nu) \left(\sin \frac{3\theta}{2} + \sin \frac{\theta}{2} \right), \\ v_e(\theta) &= -\frac{3}{8} (1-\nu) \left(\cos \frac{3\theta}{2} + \frac{\nu+7}{3\nu+5} \cos \frac{\theta}{2} \right), & v_o(\theta) &= -\frac{3}{8} (1-\nu) \left(\sin \frac{3\theta}{2} + \sin \frac{\theta}{2} \right). \end{aligned}$$

111 As well known, the squares of $\mathcal{K}_{e,o}$ are proportional to the energy release rate.

112 *2.1. Apriori asymptotic estimate of the solution components at infinity*

113 To deliver the unique solution to the problem, we demand that it decays within the supported plate as

$$w^A(r, \theta) \sim \phi^A(r, \theta) = O(r^{-5/2}), \quad \theta \in [0, \pi], \quad \text{as } r \rightarrow +\infty, \quad (18)$$

whence, by continuity, the same occurs in the free plate at $\theta = 0$. Motivation of these assumptions is given in Sec. Appendix C.1. Conversely, little knowledge is available concerning the behaviour of the solution in the free plate outside the line $\theta = 0$. For this reason, we look at some auxiliary problems which emerge from taking symmetric or anti-symmetric conditions (see Appendix Appendix A). From these, we deduce

$$w^B(r, -\pi) = W_1^\infty r + W_2^\infty + O(r^{-1/2}), \quad \text{as } r \rightarrow +\infty, \quad (19a)$$

$$\phi^B(r, -\pi) = \Psi_1^\infty \log r + \Psi_2^\infty + O(r^{-1/2}), \quad \text{as } r \rightarrow +\infty, \quad (19b)$$

114 where the constants (which may also vanish) are to be found in the following. The corresponding estimates
 115 for the jumps across the crack line easily follow, also in light of the fact that all functions vanish at infinity
 116 in the supported zone, namely

$$[[w]] = \Phi_0 x_1 - W_0^\infty + O(|x_1|^{-1/2}), \quad [[\phi]] = \Psi_0(|x_1|)^{1/2} + O(|x_1|^{-1/2}), \quad x_1 \rightarrow -\infty. \quad (20)$$

117 Furthermore, we point out that those estimates emerge by assuming the fastest growing scenario, and may
 118 well be slower than assumed, also in dependence of the applied loading. Yet, for specific external forces, these
 119 estimates may be sharpened at the expense of generality. Instead, we prefer to stick with general results to
 120 show that the solution technique does not rely on specific assumptions on the given functions.

121 For the remaining two unknowns

$$m(r, \theta) = O(r^{-5/2}), \quad v(r, \theta) = O(r^{-7/2}), \quad \theta \in (-\pi, 0), \quad \text{as } r \rightarrow +\infty. \quad (21)$$

122 Having all these information in place, we are now in position to develop solution to the problem. For this, we
 123 move to the Fourier space and use Abelian- and Tiberian-type of theorems [22] to evaluate the corresponding
 124 asymptotic behavior for the unknowns.

125 **3. Application of the Fourier transform and asymptotics of the Fourier images**

126 *3.1. Fourier analysis of the general equations*

127 In the following, we take advantage of the Fourier transform method, which has proven extremely useful
 128 in several problems dealing with continuum as well as discrete media (and even for hybrid solids, see [30]).
 129 We therefore introduce the (two-sided or bilateral) Fourier transform

$$\bar{w}(s, x_2) = \int_{-\infty}^{\infty} w(x_1, x_2) \exp(isx_1) dx_1, \quad (22)$$

130 alongside the half-transforms

$$\bar{w}^\pm(s, x_2) = \int_{-\infty}^{\infty} w_\pm(x_1, x_2) \exp(isx_1) dx_1, \quad (23)$$

131 where $w_\pm(x_1, x_2) = H(\pm x_1)w(x_1, x_2)$ and $H(x_1)$ is Heavyside's step function. Immediately, we have

$$\bar{w}(s, \cdot) = \bar{w}^+(s, \cdot) + \bar{w}^-(s, \cdot). \quad (24)$$

132 In the same way we denote the Fourier transforms of the remaining fields ϕ , m and v , noting only that, for
 133 the last, the respective integral should be treated in the sense of distributions.

134 We are now in a position to take the Fourier transform of the transmission conditions (11a,11b)

$$[[\bar{w}^+]] = [[\bar{\phi}^+]] = [[\bar{m}]] = [[\bar{v}]] = 0, \quad (25)$$

whence, clearly,

$$\llbracket \bar{w} \rrbracket = \llbracket \bar{w}^- \rrbracket, \quad \llbracket \bar{\phi} \rrbracket = \llbracket \bar{\phi}^- \rrbracket. \quad (26)$$

In similar fashion, the balance conditions (13) may be rewritten as

$$\bar{m}_0^A(0) = \bar{m}_0^B(0) = \bar{v}_0^A(0) = \bar{v}_0^B(0) = \frac{d\bar{v}_0^A}{ds}(0) = \frac{d\bar{v}_0^B}{ds}(0) = 0, \quad (27)$$

where the notation $f_0^{A,B}$ stands for

$$f_0^A(\cdot) = \lim_{x_2 \rightarrow 0^+} f^A(\cdot, x_2), \quad f_0^B(\cdot) = \lim_{x_2 \rightarrow 0^-} f^B(\cdot, x_2).$$

Besides, we recall the inverse Fourier transform

$$[w, w_+, w_-](x_1, x_2) = (2\pi)^{-1} \int_{-\infty}^{\infty} [\bar{w}, \bar{w}^+, \bar{w}^-](s, x_2) \exp(-isx_1) ds. \quad (28)$$

Taking the bilateral Fourier transform along x_1 of the first of Eqs.(3) lends a linear constant coefficient ODE whose general solution is

$$\bar{w}^A(s, x_2) = A_1 e^{-\alpha_1 x_2} + A_2 e^{-\alpha_2 x_2}, \quad \alpha_j = \sqrt{s^2 + i(-1)^j}, \quad j = 1, 2, \quad x_2 > 0, \quad (29)$$

where $A_j = A_j(s)$ and i is the imaginary unit, i.e. $i^2 = -1$. Here, provision should be taken so that the square roots lend positive real values on the real axis and branch cuts are not intersecting the real axis (for example, branch cuts may be taken parallel to the imaginary axis, see [21]). Denoting by $z^* = \Re(z) - i\Im(z)$ the complex conjugate of $z = \Re(z) + i\Im(z)$, we have

$$\alpha_1(0) = \alpha_2^*(0) = e^{-i\pi/4}, \quad (30)$$

so that $\alpha_{1,2}^2(0) = \mp i$. Similarly, the solution of the second of Eqs.(3) reads (free domain)

$$\bar{w}^B(s, x_2) = (B_1 + x_2 B_2) \exp(\beta x_2), \quad x_2 < 0, \quad (31)$$

and it is understood that $B_j = B_j(s)$ ($j = 1, 2$) and we have $\beta(s) = \sqrt{s^2}$ such that $\text{sign } s = \beta(s)/s$ for $s \in \mathbb{R}$. Moreover, to prevent having branch cuts reaching the real axis, we may perturb $\beta(s) = \lim_{\epsilon \rightarrow 0} \sqrt{s^2 + \epsilon^2}$ so that no zero sits right on the real axis [21]. With this, we are now able to introduce the splitting

$$\beta(s) = \beta^+(s)\beta^-(s), \quad \beta^+(s) = \sqrt{0 - is}, \quad \beta^-(s) = \sqrt{0 + is}, \quad (32)$$

where we take the standard definition of the square root with the cut on the negative part of real axis. It is emphasized that Fourier transforms are defined on the real axis only, but can be extended by analytic continuation into the complex plane.

In terms of the general solution, we have, in the supported plate $x_2 \geq 0$,

$$\bar{\phi}^A(s, x_2) = -\alpha_1 A_1 e^{-\alpha_1 x_2} - \alpha_2 A_2 e^{-\alpha_2 x_2}, \quad (33a)$$

$$\bar{m}^A(s, x_2) = A_1 e^{-\alpha_1 x_2} (\alpha_1^2 - \nu s^2) + A_2 e^{-\alpha_2 x_2} (\alpha_2^2 - \nu s^2), \quad (33b)$$

$$\bar{v}^A(s, x_2) = -\alpha_1 A_1 e^{-\alpha_1 x_2} (\alpha_1^2 + (\nu - 2)s^2) - \alpha_2 A_2 e^{-\alpha_2 x_2} (\alpha_2^2 + (\nu - 2)s^2), \quad (33c)$$

and in the free plate $x_2 \leq 0$

$$\bar{\phi}^B(s, x_2) = e^{\beta x_2} [\beta (B_2 x_2 + B_1) + B_2], \quad (34a)$$

$$\bar{m}^B(s, x_2) = e^{\beta x_2} [-(\nu - 1)s^2 (B_2 x_2 + B_1) + 2\beta B_2], \quad (34b)$$

$$\bar{v}^B(s, x_2) = e^{\beta x_2} [\beta(\nu - 1)s^2 (B_2 x_2 + B_1) + B_2(\nu + 1)s^2]. \quad (34c)$$

Finally, substituting (33) and (34) into the transmission conditions (25), we have:

$$\llbracket \bar{w} \rrbracket = A_1(s) + A_2(s) - \beta^{-1} B_*(s) = \llbracket \bar{w}^- \rrbracket, \quad (35a)$$

$$\llbracket \bar{\phi} \rrbracket = -\alpha_1 A_1(s) - \alpha_2 A_2(s) - B_*(s) - B_2(s) = \llbracket \bar{\phi}^- \rrbracket, \quad (35b)$$

$$0 = (\alpha_1^2 - \nu s^2) A_1(s) + (\alpha_2^2 - \nu s^2) A_2(s) + (\nu - 1)\beta B_*(s) - 2\beta B_2(s), \quad (35c)$$

$$0 = -\alpha_1(\alpha_1^2 + (\nu - 2)s^2) A_1(s) - \alpha_2(\alpha_2^2 + (\nu - 2)s^2) A_2(s) - (\nu - 1)s^2 B_*(s) - (\nu + 1)s^2 B_2(s), \quad (35d)$$

152 having introduced the convenient shorthand (see Appendix B).

$$B_*(s) \equiv \beta(s)B_1(s). \quad (36)$$

153 In the equations above (33) – (36), it is understood that $\alpha_j = \alpha_j(s)$, $\beta = \beta(s)$ and $s \in \mathbb{R}$, while (35a) and
154 (35b) can be analytically extended into the complex half-plane $s \in \mathbb{C}^-$.

155 3.2. Derivation of the Wiener-Hopf system

In light of (25), the boundary conditions (7) reads

$$\bar{m}_0^-(s) \equiv \bar{m}_0^{A,B-}(s) = \bar{M}_0^-(s), \quad (37a)$$

$$\bar{v}_0^-(s) \equiv \bar{v}_0^{A,B-}(s) = \bar{V}_0^-(s). \quad (37b)$$

156 We consider the linear system of algebraic equations (35) in the unknowns A_1, A_2, B_1, B_2 . This system
157 is regular, because its determinant has no zeros. Upon solving these unknowns in terms of $[\bar{w}^-]$ and $[\bar{\phi}^-]$
158 and then plugging the result into (37), we get the system of inhomogenous functional equations of the
159 Wiener-Hopf type

$$\begin{cases} -K_{11}[\bar{\phi}^-] + K_{12}[\bar{w}^-] = \bar{m}_0^+ + \bar{M}_0^-(s), \\ -K_{12}[\bar{\phi}^-] + s^2 K_{22}[\bar{w}^-] = \bar{v}_0^+ + \bar{V}_0^-(s), \end{cases} \quad (38)$$

where

$$\begin{aligned} \delta_0 K_{11} &= (1 - \nu)s^4 [(\alpha_1 + \alpha_2)(3 + \nu) + 2(1 + \nu)\beta] + 4(1 - \nu)s^2 \alpha_1 \alpha_2 \beta + 2\beta, \\ \delta_0 K_{12} &= s^2 \{(1 - \nu)^2 (s^2 - \alpha_1 \alpha_2) s^2 + 1 + \nu\}, \\ \delta_0 K_{22} &= \delta_0 K_{11} + i(1 - \nu)(3 + \nu)s^2 (\alpha_1 - \alpha_2), \end{aligned}$$

160 and having let

$$\delta_0(s) = (\alpha_1(s) + \beta(s))^2 (\alpha_2(s) + \beta(s))^2. \quad (39)$$

161 It is observed that, when the plate is everywhere free, that is for $\lambda \rightarrow \infty$, the system (38) decouples owing
162 to symmetry, i.e. $K_{12} \rightarrow 0$. Besides, it is $K_{11} \rightarrow K_{22}$.

163 At the origin, we have the following asymptotics for the components, that are even functions of $s \in \mathbb{R}$,

$$\left. \begin{aligned} K_{11} = K_{22} &= 2\beta(s)(1 + O(\beta(s))) \\ K_{12} &= (1 + \nu)s^2(1 + O(\beta(s))) \end{aligned} \right\} \text{as } s \rightarrow 0, \quad (40)$$

thus, by (Appendix C.13, Appendix C.36), we get asymptotic consistency at zero

$$\begin{aligned} K_{11}[\bar{\phi}^-] &= O(s^{3/2}), & K_{12}[\bar{w}^-] &= O(s^{3/2}), & \bar{m}_0^+ + \bar{M}_0^-(s) &= O(s^{3/2}), \\ K_{12}[\bar{\phi}^-] &= O(s^{5/2}), & s^2 K_{22}[\bar{w}^-] &= O(s^{5/2}), & \bar{v}_0^+ + \bar{V}_0^-(s) &= O(s^{5/2}), \end{aligned} \quad s \rightarrow 0.$$

164 We point out that individual terms at RHS of (38) have different asymptotics than their sum, namely

$$\bar{m}_0^+(s), \bar{M}_0^-(s), \bar{v}_0^+(s), \bar{V}_0^-(s) = O(1), \quad s \rightarrow 0, \quad (41)$$

165 as it appears from (Appendix C.35a, Appendix C.35b). Indeed, this result comes from the balance conditions
166 (27)

$$\bar{m}_0^+(0) + \bar{M}_0^-(0) = \bar{v}_0^+(0) + \bar{V}_0^-(0) = \frac{d\bar{v}_0^+}{ds}(0) + \frac{d\bar{V}_0^-}{ds}(0) = 0, \quad (42)$$

167 and accounting for (Appendix C.12)

$$\frac{d\bar{m}_0^+}{ds}(0) + \frac{d\bar{M}_0^-}{ds}(0) = \frac{d^2\bar{v}_0^+}{ds^2}(0) + \frac{d^2\bar{V}_0^-}{ds^2}(0) = 0. \quad (43)$$

168 At infinity we have

$$\left. \begin{aligned} K_{11} &= K_{22} = c\beta(s) + O(s^{-3}) \\ K_{12} &= \frac{1+4\nu-\nu^2}{32}s^{-2} + O(s^{-6}) \end{aligned} \right\} \text{as } |s| \rightarrow +\infty, \quad (44)$$

169 where we have let

$$c = \frac{1}{4}(1-\nu)(3+\nu). \quad (45)$$

Besides, from (Appendix C.37c, Appendix C.37d), it is

$$s\bar{m}_0^+(s) \sim \bar{v}_0^+(s) = O(s^{1/2}), \quad s\bar{M}_0^-(s) \sim \bar{V}_0^-(s) = O(s^{-\gamma_0}), \quad |s| \rightarrow \infty \text{ and } \gamma_0 > 1/2.$$

170 Thus, by (Appendix C.39), we see that diagonal terms asymptotics match that of the RHS

$$\begin{aligned} K_{11}[\bar{\phi}^-] &= O(s^{-1/2}), & K_{12}[\bar{w}^-] &= O(s^{-9/2}), & \bar{m}_0^+ + \bar{M}_0^-(s) &= O(s^{-1/2}), \\ K_{12}[\bar{\phi}^-] &= O(s^{-7/2}), & s^2K_{22}[\bar{w}^-] &= O(s^{1/2}), & \bar{v}_0^+ + \bar{V}_0^-(s) &= O(s^{1/2}), \end{aligned} \quad s \rightarrow \infty. \quad (46)$$

171 Besides, for the determinant we have

$$\Delta(s) = K_{12}^2 - s^2K_{11}K_{22} = -4cs^4\delta_0^{-1}((1-\nu^2)s^4 + 2\alpha_1\alpha_2(1-\nu)s^2 + 1), \quad (47)$$

whence

$$\Delta(s) = 4cs^4 + O(s^6), \quad s \rightarrow 0, \quad (48)$$

$$\Delta(s) = c^2s^4 + O(s^2), \quad s \rightarrow \infty. \quad (49)$$

172 Thus, the determinant of this Wiener-Hopf system tends to zero both as $s \rightarrow 0$ and as $s \rightarrow \infty$, which
173 fact suggests that the unknown quantities are not properly normalized. Consequently, in the following, we
174 transform the system (38) so that it has total index zero and both partial indices also equal to zero.

175 4. Regularization of the Wiener-Hopf system

176 Let's transform the system (38) by dividing the first equation by β and the second by $s\beta$

$$\left\{ \begin{aligned} \beta^{-1}K_{11}\bar{h}_1^- + (s\beta)^{-1}K_{12}\bar{h}_2^- &= \beta^{-1}(\bar{m}_0^+ + \bar{M}_0^-), \\ (s\beta)^{-1}K_{12}\bar{h}_1^- + \beta^{-1}K_{22}\bar{h}_2^- &= (s\beta)^{-1}(\bar{v}_0^+ + \bar{V}_0^-), \end{aligned} \right. \quad (50)$$

177 where we have let the new unknowns

$$\bar{h}_1^-(s) = -[\bar{\phi}^-], \quad \bar{h}_2^-(s) = s[\bar{w}^-].$$

For these, recalling (26) and using (Appendix C.36, Appendix C.39), we get the in their domains of analyticity:

$$\bar{h}_1^-(s) \sim \bar{h}_2^-(s) = O(s^{1/2}), \quad s \rightarrow 0, \quad (51a)$$

$$\bar{h}_1^-(s) \sim \bar{h}_2^-(s) = O(s^{-3/2}), \quad s \rightarrow \infty. \quad (51b)$$

178 Similarly, by (40),

$$\left. \begin{aligned} \beta^{-1}K_{11} &= \beta^{-1}K_{22} = 2 + O(\beta(s)), \\ (s\beta)^{-1}K_{12} &= (1+\nu)\text{sign } s + O(s), \end{aligned} \right\} \text{as } s \rightarrow 0, \quad (52)$$

whence terms in the W-H system have the following balanced asymptotics at zero

$$\left. \begin{aligned} \beta^{-1}K_{11}\bar{h}_1^-(s) &= O(s^{1/2}), & (s\beta)^{-1}K_{12}\bar{h}_2^-(s) &= O(s^{1/2}), & \beta^{-1}(\bar{m}_0^+(s) + \bar{M}_0^-(s)) &= O(s^{1/2}), \\ (s\beta)^{-1}K_{12}\bar{h}_1^-(s) &= O(s^{1/2}), & \beta^{-1}K_{22}\bar{h}_2^-(s) &= O(s^{1/2}), & (s\beta)^{-1}(\bar{v}_0^+(s) + \bar{V}_0^-(s)) &= O(s^{1/2}), \end{aligned} \right\} s \rightarrow 0.$$

179 Likewise, at infinity, we have, by (44),

$$\left. \begin{aligned} \beta^{-1}K_{11} &= \beta^{-1}K_{22} = c + O(s^{-4}), \\ (s\beta)^{-1}K_{12} &= \frac{1+4\nu-\nu^2}{32}s^{-4}\text{sign } s + O(s^{-7}\beta), \end{aligned} \right\} \text{as } |s| \rightarrow +\infty. \quad (53)$$

whereby

$$\left. \begin{aligned} \beta^{-1}K_{11}\bar{h}_1^-(s) &= O(s^{-3/2}), & (s\beta)^{-1}K_{12}\bar{h}_2^-(s) &= O(s^{-11/2}), & \beta^{-1}(\bar{m}_0^+(s) + \bar{M}_0^-(s)) &= O(s^{-3/2}), \\ (s\beta)^{-1}K_{12}\bar{h}_1^-(s) &= O(s^{-11/2}), & \beta^{-1}K_{22}\bar{h}_2^-(s) &= O(s^{-3/2}), & (s\beta)^{-1}(\bar{v}_0^+(s) + \bar{V}_0^-(s)) &= O(s^{-3/2}), \end{aligned} \right\} s \rightarrow \infty.$$

180 In anticipation of splitting plus and minus terms in (50), we need to make sure that, besides *their sum*,
181 also *each individual term at RHS* is well behaved. To this effect, we set

$$\bar{m}_*^+(s) = \bar{m}_0^+(s) + \frac{\bar{M}_0^-(0) + sq_m}{(1-is)\zeta_M}, \quad \bar{M}_*(s) = \bar{M}_0^-(s) - \frac{\bar{M}_0^-(0) + sq_m}{(1-is)\zeta_M}, \quad (54)$$

182 and

$$\bar{v}_*^+(s) = \bar{v}_0^+(s) + \frac{\bar{V}_0^-(0) + sq_{v1} + s^2q_{v2}}{(1-is)\zeta_V}, \quad \bar{V}_*(s) = \bar{V}_0^-(s) - \frac{\bar{V}_0^-(0) + sq_{v1} + s^2q_{v2}}{(1-is)\zeta_V}. \quad (55)$$

Here, $\zeta_M, \zeta_V > \gamma_0 + 2$ are some constants, to be specified later for convenience, which warrant fast enough decay at infinity. The important point here is that, with these definitions, the starred unknowns $\bar{m}_*^+(s)$ and $\bar{v}_*^+(s)$ preserve the same plus character as well as behaviour at infinity of the original variables $\bar{m}_0^+(s)$ and $\bar{v}_0^+(s)$, respectively. Furthermore, $\bar{m}_*^+(s)$ and $\bar{v}_*^+(s)$ satisfy the same balance conditions (42,43) as $\bar{m}(s)$ and $\bar{v}(s)$. This is achieved by simply letting

$$q_m = -i\zeta_M\bar{M}_0^-(0) + \frac{d\bar{M}_0^-}{ds}(0), \quad q_{v1} = -i\zeta_V\bar{V}_0^-(0) + \frac{d\bar{V}_0^-}{ds}(0), \quad (56)$$

$$q_{v2} = \frac{1}{2}\left(\zeta_V(1-\zeta_V)\bar{V}_0^-(0) - 2i\zeta_V\frac{d\bar{V}_0^-}{ds}(0) + \frac{d^2\bar{V}_0^-}{ds^2}(0)\right), \quad (57)$$

having used (42), (43) to rewrite the last terms at RHS in terms of the applied load. With such provisions and recalling (Appendix C.35), (Appendix C.37), (Appendix C.38), we obtain the asymptotics of each term

$$s\bar{m}_*^+(s), \bar{v}_*^+(s) = O(s^{5/2}), \quad s\bar{M}_*(s), \bar{V}_*(s) = O(s^3), \quad s \rightarrow 0, \quad (58a)$$

$$s\bar{m}_*^+(s), \bar{v}_*^+(s) = O(s^{-1/2}), \quad s\bar{M}_*(s), \bar{V}_*(s) = O(s^{-\gamma_0}), \quad s \rightarrow \pm\infty. \quad (58b)$$

Therefore, the W-H system now reads

$$\begin{cases} \beta^{-1}K_{11}\bar{h}_1^- + (s\beta)^{-1}K_{12}\bar{h}_2^- = \beta^{-1}(\bar{m}_*^+ + \bar{M}_*), \\ (s\beta)^{-1}K_{12}\bar{h}_1^- + \beta^{-1}K_{22}\bar{h}_2^- = (s\beta)^{-1}(\bar{v}_*^+ + \bar{V}_*), \end{cases}$$

183 that, multiplying through by β^- , becomes

$$\begin{cases} \beta^{-1}K_{11}\hat{h}_1^- + (s\beta)^{-1}K_{12}\hat{h}_2^- = \hat{m}_*^+ + \hat{M}_*, \\ (s\beta)^{-1}K_{12}\hat{h}_1^- + \beta^{-1}K_{22}\hat{h}_2^- = \hat{v}_*^+ + \hat{V}_*, \end{cases} \quad (59)$$

184 having lumped minus terms together in the new unknowns

$$\hat{h}_{1,2}^-(s) = \beta^-(s)\bar{h}_{1,2}^-(s), \quad (60)$$

185 and similarly for the plus terms at RHS

$$\hat{m}_*^+ = \frac{1}{\beta^+}\bar{m}_*^+, \quad \hat{v}_*^+ = \frac{1}{s\beta^+}\bar{v}_*^+, \quad \hat{M}_* = \frac{1}{\beta^+}\bar{M}_*, \quad \hat{V}_* = \frac{1}{s\beta^+}\bar{V}_*. \quad (61)$$

The relative estimates are easily obtained from (51) and (58),

$$\hat{h}_1^-(s), \hat{h}_2^-(s), \hat{m}_*^+(s), \hat{v}_*^+(s) = O(s), \quad s \rightarrow 0, \quad (62)$$

$$\hat{h}_1^-(s), \hat{h}_2^-(s), \hat{m}_*^+(s), \hat{v}_*^+(s) = O(s^{-1}), \quad s \rightarrow \infty, \quad (63)$$

186 while the terms representing the applied loading $\bar{M}_*(s)$ and $\bar{V}_*(s)$ behave better than the unknown functions
187 in the W-H system at both zero and infinity. As a result, we eventually arrive at the vectorial Wiener-Hopf
188 problem:

$$\mathbf{N}(s)\mathbf{H}^-(s) + \mathbf{H}^+(s) = \mathbf{F}(s), \quad (64)$$

189 where

$$\mathbf{H}^-(s) = c[\hat{h}_1^-, \hat{h}_2^-], \quad \mathbf{H}^+(s) = -[\hat{m}_*^+, \hat{v}_*^+], \quad \mathbf{F}(s) = [\hat{M}_*, \hat{V}_*], \quad (65)$$

190 and clearly

$$\mathbf{N}(s) = c^{-1} \begin{bmatrix} \beta^{-1}K_{11} & (s\beta)^{-1}K_{12} \\ (s\beta)^{-1}K_{12} & \beta^{-1}K_{22} \end{bmatrix}. \quad (66)$$

191 .

192 The matrix $\mathbf{N}(s)$ has the following asymptotics at zero

$$\mathbf{N}_0(s) = 2c^{-1} \begin{bmatrix} 1 + O(\beta) & \frac{1}{2}(1 + \nu)\frac{s}{\beta} + O(s) \\ \frac{1}{2}(1 + \nu)\frac{s}{\beta} + O(s) & 1 + O(\beta) \end{bmatrix}, \quad s \rightarrow 0, \quad (67)$$

193 and at infinity

$$\mathbf{N}_\infty(s) = \mathbf{I} + O(s^{-4}), \quad s \rightarrow \infty. \quad (68)$$

The determinant of this matrix is different from zero along the closed real axis (including infinity) and it is an even function. As a result, by Gohberg and Krein's theorem (see for example, [26]), the index of the matrix is equal to zero (ind $\det \mathbf{N} = 0$). Next, the matrix $\mathbf{N}(s)$ is symmetric and even on the main diagonal and odd on the off-diagonal terms, thus it is also positive definite. As a result, its partial indices are both equal to zero. The unknowns components asymptotics at infinity along the real axis are related to the SIFs as follows:

$$H_1^-(s), -H_1^+(s) \sim \pm 12\sqrt{\pi}e^{i\pi/4}\mathcal{K}_e \frac{c}{7+\nu}|s|^{-1}, \quad s \rightarrow \pm\infty, \quad (69a)$$

$$H_2^-(s), -H_2^+(s) \sim \pm 12\sqrt{\pi}e^{-i\pi/4}\mathcal{K}_o \frac{c}{5+3\nu}|s|^{-1}, \quad s \rightarrow \pm\infty. \quad (69b)$$

194 5. Transformation to a system of Fredholm convolution equations

195 Note that due to the estimate of the sought for solution of the W-H equation (64), there exists a vector
196 function $\mathbf{h} \in L_1(\mathbb{R})$ such that

$$\mathcal{F}\mathcal{P}_\pm \mathbf{h} = \mathbf{H}^\pm, \quad (70)$$

and this function is unique. Here, as usual, \mathcal{F} is the full Fourier transform and \mathcal{P}_\pm are the projectors defined through multiplication by the characteristic functions $H(x)$ and $1 - H(x)$ of the respective half axes \mathbb{R}_\pm . We note that $\mathcal{P}_+ + \mathcal{P}_-$ is the identity operator thus, using (70), the system (64) takes the form

$$\mathcal{F}\mathbf{h}(s) + (\mathbf{N}(s) - \mathbf{I})\mathcal{F}\mathcal{P}_- \mathbf{h}(s) = \mathbf{F}(s).$$

197 Applying now the inverse Fourier transform (28), we get

$$\mathbf{h}(\xi) + \mathcal{F}^{-1}[(\mathbf{N}(s) - \mathbf{I})\mathcal{F}\mathcal{P}_- \mathbf{h}(s)](\xi) = \mathbf{g}(\xi) \equiv \mathcal{F}^{-1}[\mathbf{F}(s)](\xi). \quad (71)$$

198 Reversing the order of the integration on application of Fubini's theorem, Eq.(71) may be rewritten as an
199 integral equation of the second kind, namely

$$\mathbf{h}(\xi) + \int_{-\infty}^0 \mathbf{K}(\xi - y)\mathbf{h}(y)dy = \mathbf{g}(\xi), \quad \xi \in \mathbb{R}, \quad (72)$$

200 where the kernel is the well defined and easily computed matrix-function

$$\mathbf{K}(\lambda) = \frac{1}{2\pi} \int_{-\infty}^{\infty} (\mathbf{N}(s) - \mathbf{I}) e^{-i\lambda s} ds.$$

Remark. Interestingly, to solve the integral equation (72) we begin by considering the half-axis $x \in \mathbb{R}_-$ and, once the solution $\mathbf{h}_*(x)$ is obtained there, it may be extended to the positive half-axis by direct computation, in a sort of post-processing stage, through

$$\mathbf{h}(\xi) = \mathbf{g}(\xi) - \int_{-\infty}^0 \mathbf{K}(\xi - y) \mathbf{h}(y) dy, \quad \xi \in \mathbb{R}_+.$$

201 In contrast, when considering the classical approach to systems of integral equations defined on either half
202 axis, one moves in the opposite direction to reduce it in Wiener-Hopf form, namely one needs to introduce
203 an auxiliary function on the other half-axis and then one transforms the system to have a difference kernel.

To establish a link between the solution of the system of integral equations (72) and the SIFs we integrate by parts

$$\begin{aligned} H^- &= \int_{-\infty}^0 h(x) e^{isx} dx = \frac{h(x)}{is} e^{isx} \Big|_{-\infty}^0 - \frac{1}{is} \int_{-\infty}^0 \frac{dh}{dx}(x) e^{isx} dx = \mp i h(0) |s|^{-1} + o(s^{-1}), \quad s \rightarrow \pm\infty, \\ H^+ &= \int_0^{\infty} h(x) e^{isx} dx = \frac{h(x)}{is} e^{isx} \Big|_0^{\infty} - \frac{1}{is} \int_0^{\infty} \frac{dh}{dx}(x) e^{isx} dx = \pm i h(0) |s|^{-1} + o(s^{-1}), \quad s \rightarrow \pm\infty, \end{aligned}$$

204 and, upon recalling asymptotic relationships (69), we get the sought for relationships:

$$h_1(0) = -12e^{-i\pi/4} \frac{c\sqrt{\pi}}{7+\nu} \mathcal{K}_e, \quad h_2(0) = 12e^{i\pi/4} \frac{c\sqrt{\pi}}{5+3\nu} \mathcal{K}_o. \quad (73)$$

205 6. Numerical solution

206 Let us assume for the dimensionless crack loading

$$M_0(x_1) = \frac{\lambda M_y^d}{D} = C_m \zeta f_m(-\zeta x_1), \quad V_0(x_1) = \frac{\lambda^2 V_y^d}{D} = C_v \zeta^2 f_v(-\zeta x_1), \quad x_1 < 0, \quad (74)$$

207 where M_y^d and V_y^d are the *dimensional* bending moment and shearing force applied at the crack line in terms
208 of the dimensional coordinate x

$$M_y^d = Q_m f_m \left(-\frac{x}{x_0} \right), \quad V_y^d = Q_v f_v \left(-\frac{x}{x_0} \right), \quad x < 0. \quad (75)$$

209 Clearly, the constants Q_m and Q_v have dimensions of force and force over length, respectively, and they
210 are brought in dimensionless form as $C_m = Q_m x_0 D^{-1}$ and $C_v = Q_v x_0^2 D^{-1}$. Here, we have introduced the
211 dimensionless parameter ζ

$$\lambda = x_0 \zeta, \quad \text{or, equivalently,} \quad k = \frac{D}{x_0^4} \zeta^{-4} \equiv k_0 \zeta^{-4}, \quad (76)$$

212 $x_0 > 0$ being a reference length. We point out that, due to the introduced normalisation, the original
213 dimensional stress intensity factors K_e^d , K_o^d are related to their dimensionless counterparts through

$$\frac{\sqrt{x_0}}{D} K_e^d = \zeta^{-1/2} \mathcal{K}_e(\zeta), \quad \frac{\sqrt{x_0}}{D} K_o^d = \zeta^{-1/2} \mathcal{K}_o(\zeta). \quad (77)$$

214 In the following, we consider two cases, namely $C_m = 1$, $C_v = 0$ and $C_m = 0$, $C_v = 1$.

215 6.1. Bending moment applied to the crack faces ($C_m = 1, C_v = 0$)

216 We first consider the following function in (75)

$$f_m(t) = t^{n_m} e^{-t}.$$

217 By applying the Fourier transform we obtain

$$\bar{M}_0^-(s) = \frac{\zeta^{n_m+1} \Gamma(n_m + 1)}{(\zeta + is)^{n_m+1}}, \quad (78)$$

218 while the Mellin transform lends

$$\tilde{M}_0(s) = \int_0^\infty r^{s+1} \zeta^{n_m+1} r^{n_m} e^{-\zeta r} dr = \frac{1}{\zeta^{s+1}} \Gamma(s + n_m + 2). \quad (79)$$

Note that $\bar{M}_0(0) = \tilde{M}_0(-1) = \Gamma(n_m + 1) \neq 0$ independent of ζ . This behavior warrants that the displacement $w_0^B(x_1)$ in the free plate grows linearly to infinity along the crack line, i.e. as $x_1 \rightarrow -\infty$. After the transformations of Eqs.(54,61), one finds

$$\hat{M}_* = \frac{\zeta^{n_m+1} \Gamma(n_m + 1)}{\beta_+(s)} \left(\frac{1}{(\zeta + is)^{n_m+1}} - \frac{1}{(1 - is)^{\xi_M} \zeta^{n_m+1}} + i \frac{s(\zeta \xi_M + n_m + 1)}{(1 - is)^{\xi_M} \zeta^{n_m+2}} \right).$$

219 Hereinafter, for the numerics, we take

$$\nu = 0.25, \quad n_m = 4, \quad n_v = 3, \quad \xi_M = \xi_v = 7. \quad (80)$$

220 Owing to the absence of the shearing force, the second component of the vector from the right-hand side
 221 of the system of integral equations (72), namely $g_2(\xi)$, equals zero, while the first component, $g_1(\xi)$, can
 222 be computed in closed form, as presented in Sec.Appendix B.1. However, it was not possible to obtain
 223 an analytical representation for the kernel $\mathbf{K}(\xi)$, which is therefore computed numerically. As discussed in
 224 Section 5, we first compute the solution on the negative ξ -axis and then reconstruct it on the positive axis.
 225 Since the system is well defined and the projection methods converge [26], we reduce the infinite domain of
 226 integration to a finite one through controlling the behaviour of the solution at infinity. Computations are
 227 carried out on a finite grid of points whose density guarantees that the relative error is of the order of 10^{-4} .

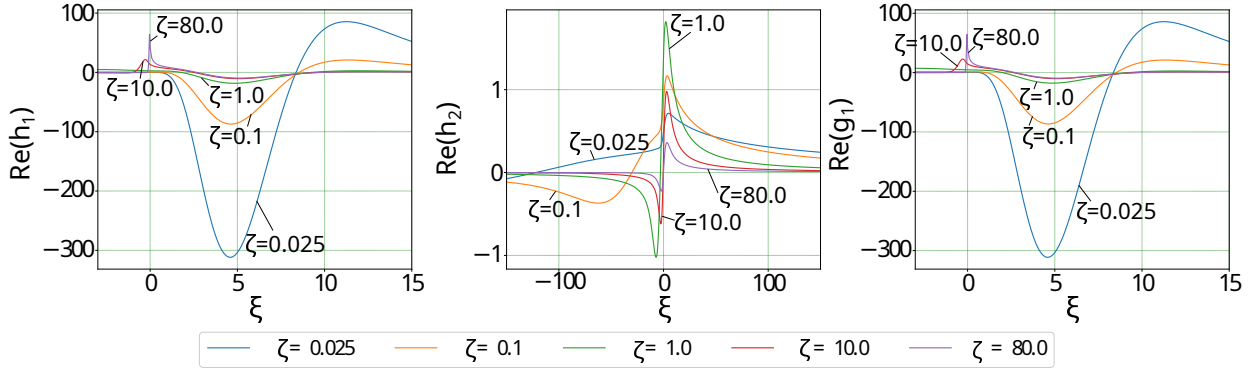


Figure 4: Numerical solution of the system of integral equations (72), in the absence of shearing force, for different values of the Winkler parameter $k = k_0 \zeta^{-4}$ (compare (76)). It appears that the first solution component, h_1 , is very close to the right hand side already, while the contribution from h_2 is negligible.

228 Figure 4 shows the real part of the components in the unknown vector $\mathbf{h}(\xi)$ as well as the nonzero right-
 229 hand side $g_1(\xi)$ for the system of the integral equations (72). Interestingly, the first component $h_1(\xi)$ is very
 230 similar to the right-hand side $g_1(\xi)$, while the second component $h_2(\xi)$ is 2 order of magnitude smaller. This
 231 means that, within this loading, the system is almost symmetric and the numerical system diagonal. Clearly,
 232 results depend significantly on the Winkler parameter, especially near the crack-tip.

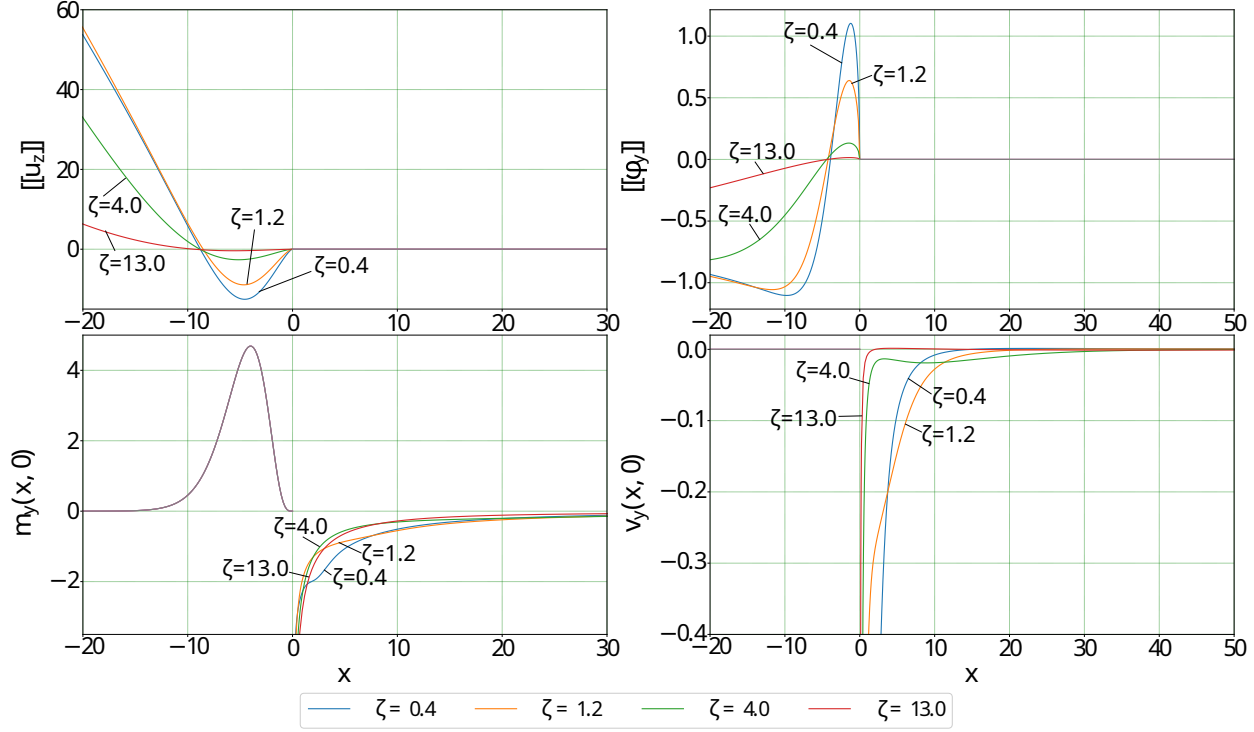


Figure 5: Jump of the displacement and rotation, bending moment and shearing force along the crack line $y = 0$ where a distribution of bending moment is applied, in the absence of shearing force, i.e. $V_0 \equiv 0$. The dimensional coordinate x is used as the abscissa to bring about the role of the foundation through ζ .

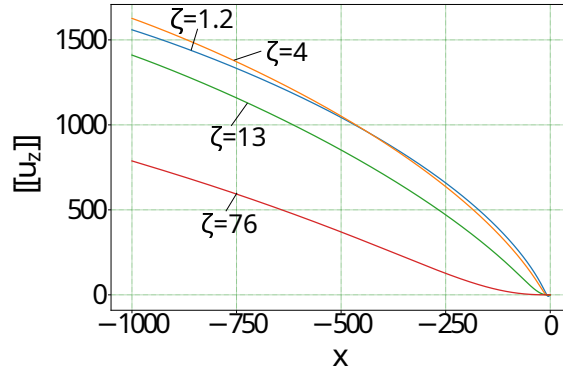


Figure 6: Far-field behavior of the jump of the displacement along the crack surfaces for the case of bending moment, i.e. $V_0 \equiv 0$.

233 Figure 5 illustrates the mechanical unknowns over the line $y = 0$ (that is along the crack surfaces and
 234 at the interface between the supported and the unsupported plate). It is emphasized that the jump of the
 235 displacement and slope is identically zero beyond the crack-tip ($x > 0$), while the bending moment and
 236 shearing force correspond to the applied load on the crack line ($x < 0$).

237 To highlight the behaviour of the solution in the far-field, Figure 6 presents the jump of the displacement
 238 on a wider interval. Here, we observe a linear growth of the displacement at infinity (compare (20)) for large
 239 value of ζ (small k). On the other hand, for small values of ζ , square root growth represents the dominant
 240 asymptotics, that is related to the skew-symmetric part of the solution. This is in the agreement with the
 241 analysis provided in Appendix A (see Table A.1) and is a direct consequence of the condition $\tilde{M}_0(-1) \neq 0$.

242 Finally, Figure 7 shows the normalised SIFs as functions of the Winkler parameter ζ , as computed

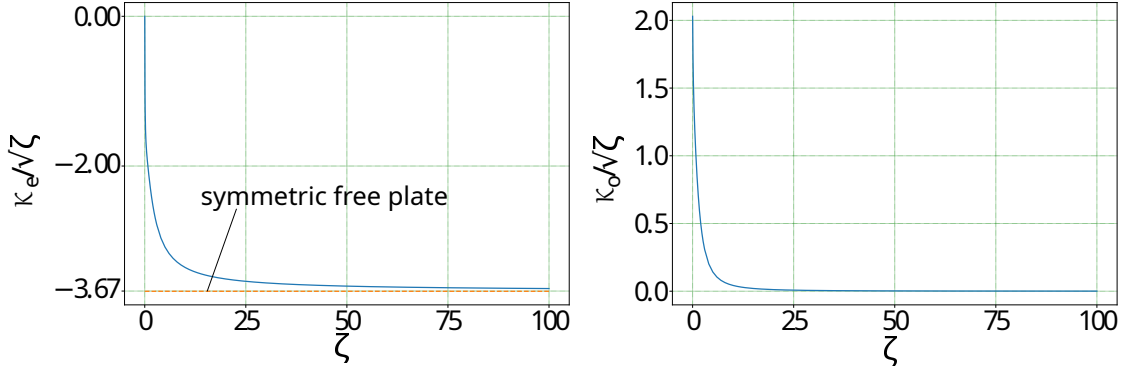


Figure 7: Normalised stress intensity factors $\zeta^{-1/2}\mathcal{K}_e(\zeta)$ and $\zeta^{-1/2}\mathcal{K}_o(\zeta)$ (compare (77)) as functions of the auxiliary parameter ζ representing changes in the Winkler parameter k (see (76)): Case of applied bending moment, i.e. $V_0 \equiv 0$. The horizontal dashed line corresponds to $\zeta^{-1/2}\mathcal{K}_e$ for a free plate under symmetric conditions, see (Appendix A.9).

243 through the relationships (73). In particular, the limiting value of \mathcal{K}_e as $\zeta \rightarrow \infty$ matches the corresponding
 244 SIF obtained setting $\nu = 0.25$ in (Appendix A.9), namely $\mathcal{K}_e\zeta^{-1/2} = -3.67085$. This appears in the Fig.7
 245 as a horizontal asymptote. A curve fitting by the Least Square (LSQ) method for $\mathcal{K}_e(\zeta)\zeta^{-1/2}$ on the interval
 246 $\zeta = [65, 100]$ is given by $\mathcal{K}_e(\zeta)\zeta^{-1/2} \approx -3.668977 + 3.237402\zeta^{-1}$ as $\zeta \rightarrow \infty$, with relative error of $5.1e - 04$,
 247 that is consistent with the accuracy achieved when computing the solution of the system of the integral
 248 equations.

249 6.2. Shearing force applied to the crack faces ($C_m = 0$, $C_v = 1$)

In this case, we take $g_1 \equiv 0$ and $g_2(x) = i\mathcal{F}^{-1}[\hat{V}_*(s)](x)$ as the right hand side of the system of integral equations (72). Consequently, it is

$$\bar{V}_0^-(s) = is\bar{M}_0^-(s),$$

250 where the function $\bar{M}_0(s)$ is defined in (78). It is easy to see that the condition $\bar{V}_0^-(0) = 0$ is satisfied
 251 automatically. The original function (after normalisation) takes the form

$$V_0(x_1) = \zeta^{n_v+1}(\zeta x_1 + n_v)(-x_1)^{n_v-1}e^{\zeta x_1}. \quad (81)$$

252 and its Mellin transform is

$$\tilde{V}_0^-(s) = -\frac{2+s}{\zeta^{s+1}}\Gamma(n_v + s + 2). \quad (82)$$

253 Hereinafter, we assume $\xi_v = 6$.

254 The counterparts of Figures 4–7 are presented in Figures 8–11, this time for shearing force, i.e. $M_0 \equiv 0$.
 255 In particular, Figure 8 reveals that $h_2(\xi)$ is really the dominating component of the solution, with a small
 256 contribution from $h_1(\xi)$, which fact suggests that the loading condition is close to skew-symmetry.

257 Figure 9 presents the mechanical unknowns for the case when a shearing force is applied. Once again we
 258 see that no jump of displacement and slope occurs beyond the crack-tip ($x > 0$), while the applied loading
 259 appears along the crack faces ($x < 0$).

260 To highlight the behaviour of the solution in the far field, e.g. as $x \rightarrow -\infty$, Figure 10 presents the
 261 jump of the displacement and of the slope on a wide interval. Here, we observe square root growth of the
 262 displacement at infinity (compare (20)) for large ζ (small k). On the other hand, for small ζ (large k), the
 263 displacement tends to the symmetric part of the solution and grows linearly. This again is in the agreement
 264 with the limiting analysis provided in Appendix A (see Table A.1) and is a direct consequence that the
 265 condition $\tilde{V}_0(-1) \neq 0$.

266 As it can be seen in Figure 11, the normalised SIF $\mathcal{K}_o\zeta^{-1/2}$ asymptotes, as $\zeta \rightarrow \infty$, to the limiting case of a
 267 free plate under skew-symmetric conditions, given in (Appendix A.6) (see Appendix A). The corresponding
 268 horizontal asymptote is drawn in the picture. Comparing this limiting value, $\mathcal{K}_o\zeta^{-1/2} = 0.831818$, with the
 269 approximated SIF computed from the solution of the system of integral equations provides the relative error
 270 of the order of $3.6 \cdot 10^{-4}$, that again is consistent with the accuracy of the computations.

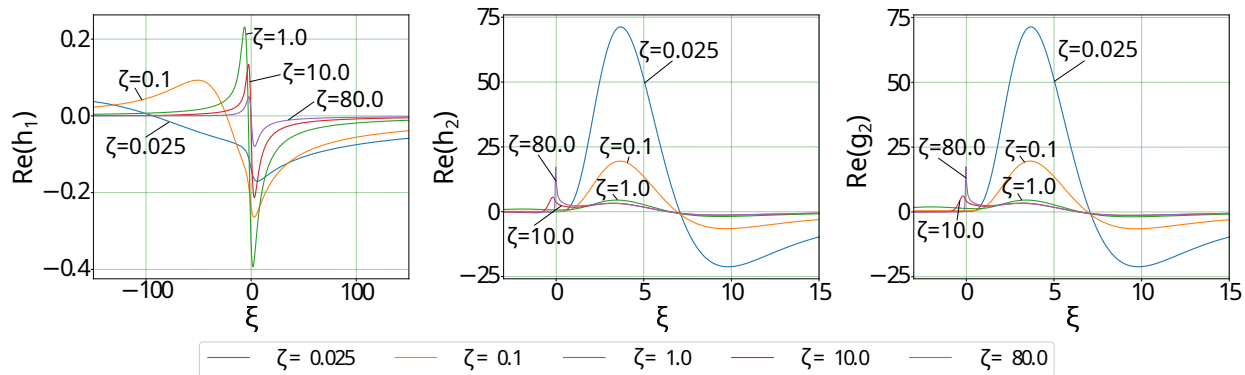


Figure 8: Numerical solution of the system of the integral equations (72) in case of applied shear force for various values of the Winkler parameter $k = k_0 \zeta^{-4}$ (compare (76)). The first two graphs correspond to the two components of the solution, while the third one represents the nonzero component at the right hand side.

7. Conclusions

In this paper, we consider the Linear Elastic Fracture Mechanics (LEFM) problem of a thin Kirchhoff plate partially supported by a Winkler foundation, in an attempt to incorporate the role of the support in any model related to sheet cutting. Indeed, almost any (possibly nonlinear) thermo-mechanical dissipative model of cutting, at some stage, takes into consideration the LEFM stress intensity factors (SIFs). In fact, our deepest motivation lies in the observation that providing good mechanical constraining conditions is crucial for any quality cutting process. The Kirchhoff plate is endowed with a semi-infinite rectilinear crack that sits right at the boundary of the supported zone. As a result, the problem is no longer symmetric even locally, in the neighborhood of the crack-tip. The problem is first formulated in terms of a pair of coupled functional equations of the Wiener-Hopf type, whose kernel cannot be factored in general. To circumvent this shortcoming, the problem is then recast in terms of a pair of integral equations on a half-domain, which are then easily solved numerically. However, to guarantee that the numerical solution is meaningful, the problem structure is manipulated and regularized, taking advantage of the features of the mechanical setup, mostly the global equilibrium conditions in the free (unsupported) plate.

The resulting numerical system is very stable and may be efficiently computed. The numerical solution reveals that the supporting condition is very relevant in determining (a) the fields in the neighborhood of the crack-tip and (b) their asymptotic value in far-field on the crack line. Indeed, while the observation (a) is consistent with the intuition and with the fact that stable cutting requires solid support, finding (b) is somewhat surprising because it reveals that little support imperfections may be amplified in the far-field behaviour of the free plate. In fact, we show how the loading properties determine the far-field behaviour. Besides, we show that, for the limiting situation of an exceedingly stiff support and in dependence of the applied loading, SIFs converge to the case of a free plate in either symmetric or skew-symmetric deformation, or, in general, to a linear combination thereof.

Contrarily to intuition, in neither case the situation of a clamped plate is retrieved, because it possesses a different decay rate in the neighborhood of the crack tip. In general, we find that both symmetric and skew-symmetric SIFs appear simultaneously, which depend on the support stiffness in opposing fashion, namely one increases while the other decreases. As a result, although no optimal support stiffness may be envisaged, it is deduced that the role of the support is to couple the symmetric and the skew-symmetric part of the solution. Therefore, the nature of the support affects the failure mode in a fundamental manner, and it is capable of shifting failure from mode II (bending) to mode III (shear). This observation may produce far reaching consequences, once it is associated with the fact that, in general, materials behave in a very different manner when subjected to different failure modes (e.g. in shear or bending).

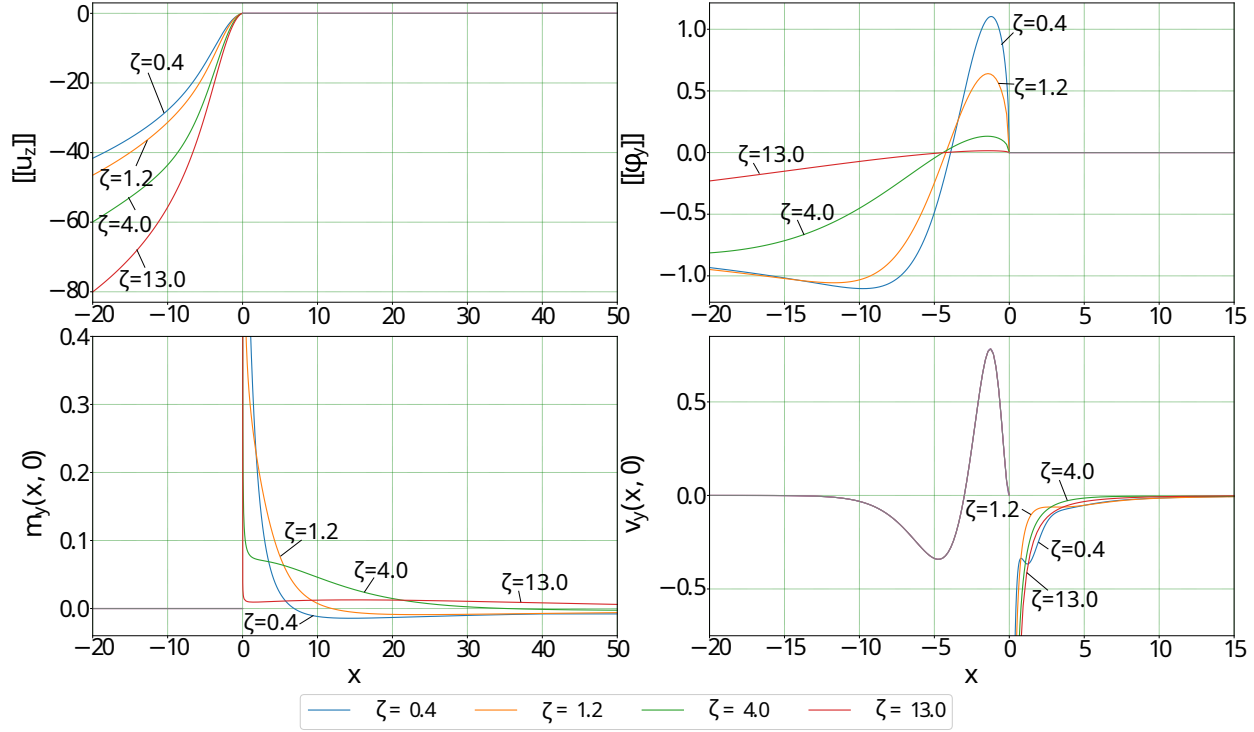


Figure 9: Jump of the displacements and of the rotations, bending moment and shearing force on the line $x_2 = 0$ for the case of applied shearing force ($M_0 \equiv 0$).

303 Acknowledgments

304 Authors gratefully acknowledge funding from the European Union's Horizon 2020 MSCA-RISE-2020,
 305 Research and Innovation Staff Exchange, under the H2020-EU.1.3. - EXCELLENT SCIENCE - Marie
 306 Skłodowska-Curie Actions Main Programme, grant agreement No 101008140, EffectFact. GM is grateful
 307 for a three month visiting position at the University of Modena and Reggio Emilia, under the long-term
 308 visiting programme, in 2022. AN acknowledges support from the National Group of Mathematical Physics
 309 (GNFM), within the Institute of Higher Mathematics (INDAM). AN also gratefully mentions support from
 310 Mathematics for Industry 4.0 (Math4I4), under the PRIN scheme.

311 Declaration of generative AI in scientific writing

312 Authors have not taken advantage of AI in their scientific writing

313 Appendix A. Limiting problems

314 *Exceedingly weak foundation*

When the stiffness of the support is exceedingly weak ($k \rightarrow 0$), the corresponding solution for a free plate loaded along the crack surfaces can be found in closed form and it will be a combination of two fundamental solutions, symmetric or skew-symmetric, in dependence of the prescribed loading. On the other hand, when the stiffness of the foundation becomes infinite $k \rightarrow \infty$ ($\varpi \rightarrow 0$), the plate becomes fixed on the crack line beyond the crack tip. Again, the solution is obtained by combining the symmetric and skew-symmetric fundamental loading conditions. In either case, solutions may be readily found in terms of Mellin transforms

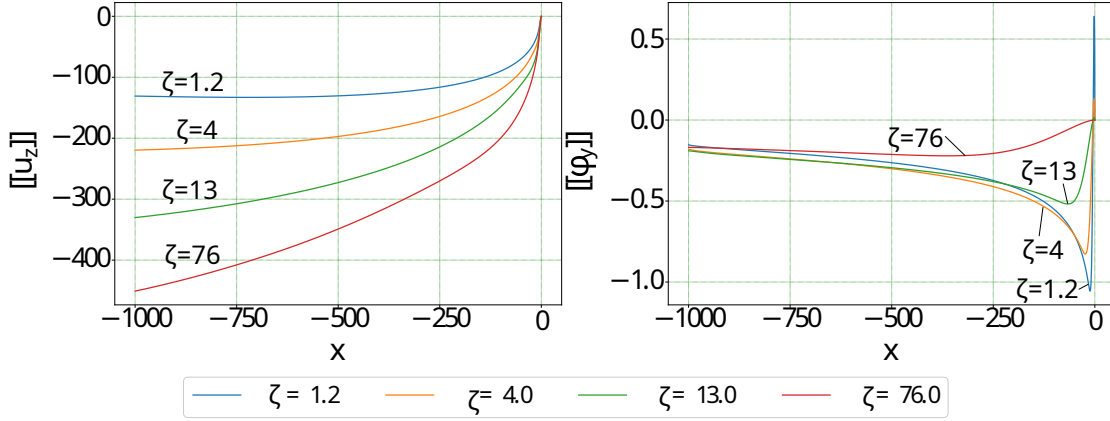


Figure 10: Jumps of the displacement and of the slope across the crack line plotted on wider range to capture the far-field asymptotics, for the case of $M_0 \equiv 0$.

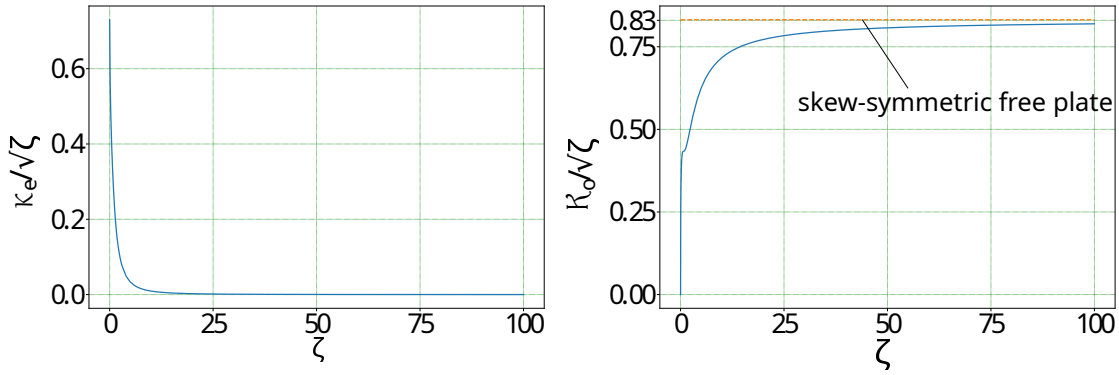


Figure 11: Normalised stress intensity factors $\zeta^{-1/2}\mathcal{K}_e(\zeta)$ and $\zeta^{-1/2}\mathcal{K}_o(\zeta)$ (compare (77)) as functions of the auxiliary parameter ζ representing changes in the Winkler parameter k (see (76)): Case of applied shearing force, i.e. $M_0 \equiv 0$. Clearly, the limit of an exceedingly stiff foundation lends the SIF for a skew-symmetric free plate

(hereinafter denoted by an overtilde),

$$\tilde{w}_0^-(s) = \int_0^\infty r^{s-1} w(r, -\pi) dr, \quad \tilde{\phi}_0^-(s) = \int_0^\infty r^s \phi(r, -\pi) dr, \quad (\text{Appendix A.1a})$$

$$\tilde{m}_0^-(s) = \int_0^\infty r^{s+1} m(r, -\pi) dr, \quad \tilde{v}_0^-(s) = \int_0^\infty r^{s+2} v(r, -\pi) dr, \quad (\text{Appendix A.1b})$$

suitably defined to have the same strip of analyticity for all functions. The inverse of Mellin is accordingly defined as

$$w(r, -\pi) = \frac{1}{2\pi i} \int_{c-i\infty}^{c+i\infty} r^{-s} \tilde{w}_0^-(s) ds, \quad \phi(r, -\pi) = \frac{1}{2\pi i} \int_{c-i\infty}^{c+i\infty} r^{-s-1} \tilde{\phi}_0^-(s) ds, \quad (\text{Appendix A.2a})$$

$$m(r, -\pi) = \frac{1}{2\pi i} \int_{c-i\infty}^{c+i\infty} r^{-s-2} \tilde{m}_0^-(s) ds, \quad v(r, -\pi) = \frac{1}{2\pi i} \int_{c-i\infty}^{c+i\infty} r^{-s-3} \tilde{v}_0^-(s) ds. \quad (\text{Appendix A.2b})$$

315 We look for solutions which abide by the zero asymptotics (14), whence

$$-\frac{3}{2} < \Re(s) < \Re(s_*). \quad (\text{Appendix A.3})$$

316 *Skew-symmetric cracked free plate*

We now consider a skew-symmetric problem along the crack line for a free plate, whence $w_0^+ = m_0^+ \equiv 0$. This solution is given by

$$\tilde{w}_0^-(s) = \frac{-(1+\nu)}{(3+\nu)(1-\nu)s(s+1)}\tilde{M}_0(s) + \frac{2\tan(\pi s)}{(3+\nu)(1-\nu)s(s+1)(s+2)}\tilde{V}_0(s), \quad (\text{Appendix A.4})$$

$$\tilde{\phi}_0^-(s) = \frac{-2\cot(\pi s)}{(3+\nu)(1-\nu)(s+1)}\tilde{M}_0(s) + \frac{(1+\nu)}{(3+\nu)(1-\nu)(s+1)(s+2)}\tilde{V}_0(s). \quad (\text{Appendix A.5})$$

317 For $\tilde{V}_0(s) \equiv 0$, if we have the balance condition $\tilde{M}_0(-1) = 0$ due to symmetry, then $\Re(s) < 0$, and the
 318 behaviour at infinity of $w_0^-(r)$ is $O(1)$. Similarly, we have $\phi_0^-(r) = O(1)$ at infinity. Conversely, assuming
 319 $\tilde{M}_0(-1) \neq 0$, we have $\Re(s) < -1$ and $w_0^-(r) = O(r)$ and $\phi_0^-(r) = O(\ln(r))$ at infinity. Analysing behaviour
 320 of the solution near the point $s = -3/2$ we conclude that in this case both SIFs are equal to zero:

$$\mathcal{K}_o = \mathcal{K}_e = 0.$$

321 For $\tilde{M}_0(s) \equiv 0$, we have $-3/2 < \Re(s) < -1/2$, and the behaviour at infinity of $w_0^-(r)$ is $O(r^{1/2})$. Conversely,
 322 for $\tilde{\phi}_0^-(s)$, it is $\Re(s) < +\infty$ assuming the skew-symmetric equilibrium condition $\tilde{V}_0(-1) = 0$, whence $\phi_0^-(r)$
 323 behaves like $V_0(r)$ at infinity. If, instead, $\tilde{V}_0(-1) \neq 0$, we have $\phi_0^-(r) = O(1)$ at infinity.

324 Finally, computing the residue of $\tilde{w}(s, \theta)$ at $s = -3/2$, we find

$$w(r, \theta) = \mathcal{K}_o w_o(\theta) r^{3/2} + O(r), \quad \text{as } r \rightarrow 0,$$

325 which matches the asymptotic analysis (14) and provides the displacement intensity factor

$$\mathcal{K}_o = -i \frac{4(3\nu+5)}{3(\nu+3)(1-\nu)} \tilde{V}_0(-3/2), \quad \mathcal{K}_e = 0. \quad (\text{Appendix A.6})$$

326 *Symmetric cracked free plate*

The symmetric solution whereby $\phi_0^+ = v_0^+ = 0$ lends

$$\tilde{w}_0^-(s) = \frac{(1+\nu)}{(3+\nu)(1-\nu)s(s+1)}\tilde{M}_0(s) - \frac{2\cot(\pi s)}{(3+\nu)(1-\nu)s(s+1)(s+2)}\tilde{V}_0(s), \quad (\text{Appendix A.7})$$

$$\tilde{\phi}_0^-(s) = \frac{2\tan(\pi s)}{(3+\nu)(1-\nu)(s+1)}\tilde{M}_0(s) + \frac{(1+\nu)}{(3+\nu)(1-\nu)(s+1)(s+2)}\tilde{V}_0(s). \quad (\text{Appendix A.8})$$

327 Again, we first consider the case $\tilde{V}_0(s) \equiv 0$ and observe that, for w_0^- , we find no poles assuming the
 328 equilibrium condition $\tilde{M}_0(-1) = 0$ and it follows that $w_0^-(r)$ behaves just like $M_0(r)$ does as r tends to
 329 infinity. Conversely, assuming $\tilde{M}_0(-1) \neq 0$, we have $\Re(s) < -1$ and $w_0^-(r) = O(r)$ at infinity. For $\phi_0^-(r)$ we
 330 have $\Re(s) < -1/2$ and $\phi_0^-(r) = O(r^{-1/2})$ at infinity. The residue of w at $s = -3/2$ lends

$$\mathcal{K}_e = -2i \frac{\nu+7}{3(1-\nu)(\nu+3)} \tilde{M}_0(-3/2), \quad \mathcal{K}_o = 0. \quad (\text{Appendix A.9})$$

331 In case $\tilde{M}_0(s) \equiv 0$, we have $\Re(s) < -1$ and $w_0^-(r) = O(\ln r)$ as r goes to infinity. If $\tilde{V}_0(-1) = 0$, $\phi_0^-(r)$
 332 behaves like $V_0(r)$ at infinity, otherwise $\phi_0^-(r) = O(1)$. In this case both SIFs are zeros.

333 The following table collects information on the behaviour of all possible solutions at infinity.

334 *Half-plate clamped and cracked along the boundary*

We consider an infinite half-plate, with a rectilinear boundary at $x_2 = 0$. The plate is clamped along this boundary for $x_1 > 0$, and it is cracked for $x_1 < 0$. Demanding $w = \phi = 0$ for $x_1 > 0$, one gets

$$\tilde{w}_0^-(s) = \frac{2(1+\nu)\tilde{M}_0 \sin^2(\pi s)}{s(s+1)\Delta_{cl}(s)} + \frac{2\tilde{V}_0 \sin(2\pi s)}{s(s+1)(s+2)\Delta_{cl}(s)}, \quad (\text{Appendix A.10})$$

$$\tilde{\phi}_0^-(s) = \frac{2\tilde{M}_0 \sin(2\pi s)}{(s+1)\Delta_{cl}(s)} - \frac{2(1+\nu)\tilde{V}_0 \sin^2(\pi s)}{(s+1)(s+2)\Delta_{cl}(s)}, \quad (\text{Appendix A.11})$$

| | | |
|----------------|---|--|
| skew-symmetric | $\tilde{V}_0(s) \equiv 0$ | $\tilde{M}_0(s) \equiv 0$ |
| $w_0^-(r)$ | $O(1)$ if $\tilde{M}_0(-1) = 0$, $O(r)$ otherwise | $O(r^{-1/2})$ if $\tilde{V}_0(-1/2) = 0$, $O(\sqrt{r})$ otherwise |
| $\phi_0^-(r)$ | $O(1)$ if $\tilde{M}_0(-1) = 0$, $O(\ln(r))$ otherwise | $V_0(r)$ if $\tilde{V}_0(-1) = 0$, $O(1)$ otherwise |
| symmetric | $\tilde{V}_0(s) \equiv 0$ | $\tilde{M}_0(s) \equiv 0$ |
| $w_0^-(r)$ | $O(1)$ if $\tilde{M}_0(-1) = 0$, $O(r)$ otherwise | $O(1)$ if $\tilde{V}_0(-1) = 0$, $O(\ln r)$ otherwise |
| $\phi_0^-(r)$ | $O(1/\sqrt{r})$ | $V_0(r)$ if $\tilde{V}_0(-1) = 0$, $O(1)$ otherwise |

Table A.1: Behaviour of the solutions of the limiting problems as $r \rightarrow \infty$

335 where

$$\Delta_{cl}(s) = 4 + (3 - \nu)^2 + (1 - \nu)(3 + \nu) \cos(2\pi s).$$

336 The first pole of this solution is located at $s = -3/2 \pm i\varepsilon$, where

$$\varepsilon = \frac{1}{2\pi} \cosh^{-1} \left(\frac{4 + (3 - \nu)^2}{(1 - \nu)(3 + \nu)} \right) > 0.$$

337 Thus, the singularity in the displacement takes the form

$$w(r, \theta) = O(r^{3/2 \mp i\varepsilon}), \quad \text{as } r \rightarrow 0,$$

338 which does not match the singularity of the problem in the presence of a foundation, no matter how stiff.
339 Interestingly, a recent paper [11] has been devoted to analysis of the stress singularity for a partially clamped
340 plate with a crack on the boundary exhibiting surface stress effects.

341 Appendix B. Forcing terms in the system of integral equations

342 Appendix B.1. Bending moment

$$g_1(x) = \mathcal{F}^{-1}[\hat{M}_*(s)](x) = \begin{cases} \frac{\zeta^{n_m+1} \sqrt{2}}{1+i} (-x)^{n_m+\frac{1}{2}} e^{\zeta x} U\left(\frac{1}{2}, \frac{3}{2} + n_m, -\zeta x\right), & x < 0, \\ \frac{\sqrt{2} \Gamma(n_m+1)}{1+i} \left(\sqrt{\frac{\zeta}{\pi}} U\left(\frac{1}{2}, \frac{1}{2} - n_m, \zeta x\right) - \frac{x^{\xi_M - \frac{1}{2}}}{\Gamma(\xi_M + \frac{1}{2})} M\left(\xi_M, \xi_M + \frac{1}{2}, -x\right) - \right. \\ \left. \frac{(2\xi_M - 1)(n_m + \zeta \xi_M + 1) \Gamma(\frac{1}{2} - \xi_M)}{2\pi \zeta} \cos(\pi \xi_M) x^{\xi_M - \frac{3}{2}} M\left(\xi_M, \xi_M - \frac{1}{2}, -x\right) \right), & x > 0, \end{cases} \quad (\text{Appendix B.1})$$

343 where $M(a, b, c)$ is Kummer's and $U(a, b, c)$ Tricomi's (confluent hypergeometric) function (for the definitions,
344 see [12]).

345 Appendix C. Asymptotics of the solution components in the frequency domain

346 Appendix C.1. Asymptotic behavior at $s = 0$

347 Appendix C.1.1. Analysis of the balance conditions

348 The notation (36) is motivated by the following analysis which demonstrates that

$$A_j(0) = B_j(0) = 0.$$

349 Indeed, rewriting (27) through (33), we get, for the supported plate, an homogeneous systems of three linear
 350 equations in the unknowns A_j , namely

$$\lim_{s \rightarrow 0} [A_1 (\alpha_1^2 - \nu s^2) + A_2 (\alpha_2^2 - \nu s^2)] = 0,$$

$$\lim_{s \rightarrow 0} [\alpha_1 A_1 (\alpha_1^2 + (\nu - 2)s^2) + \alpha_2 A_2 (\alpha_2^2 + (\nu - 2)s^2)] = 0,$$

$$\lim_{s \rightarrow 0} \frac{d}{ds} \left(\alpha_1 A_1 (\alpha_1^2 + (\nu - 2)s^2) + \alpha_2 A_2 (\alpha_2^2 + (\nu - 2)s^2) \right) = 0.$$

353 Recalling (30), we observe that the first pair of equations provide a regular system with determinant $(\alpha_2(0) -$
 354 $\alpha_1(0))\alpha_1^2(0)\alpha_2^2(0) \neq 0$, whence $A_j(0) = 0$, ($j = 1, 2$). Consequently, alongside the balance conditions (27),
 355 we have

$$\bar{w}_0^A(0) = \bar{\phi}_0^A(0) = 0. \quad (\text{Appendix C.1})$$

356 The last equation gives immediately

$$\lim_{s \rightarrow 0} [\alpha_1^3(0)A_1'(s) + \alpha_2^3(0)A_2'(s)] = 0,$$

357 whence, by (30),

$$A_1'(s) = iA_2'(s) + O(|s|), \quad s \rightarrow 0. \quad (\text{Appendix C.2})$$

358 In terms of asymptotic estimates, this gives either ($j = 1, 2$)

$$A_j(s) \sim a_j s^\varpi, \quad a_1 = ia_2, \quad s \rightarrow 0, \quad 0 < \varpi \leq 1, \quad (\text{Appendix C.3})$$

359 that will be proved incorrect in Eq.(Appendix C.17), or

$$A_j(s) \sim a_j s^{\varpi_j}, \quad s \rightarrow 0, \quad \varpi_j > 1, \quad (\text{Appendix C.4})$$

360 with a_1 and a_2 complex-valued constants. The same path of reasoning may be carried out for $B_j(s)$, but we
 361 choose to follow another approach.

362 *Appendix C.1.2. Connecting B_* , B_2 to the transforms \bar{m}_0 and \bar{v}_0*

Specializing (34) to the crack line and accounting for (36), one finds

$$\bar{m}_0 = -(\nu - 1)\beta B_* + 2\beta B_2, \quad (\text{Appendix C.5a})$$

$$\bar{v}_0 = (\nu - 1)s^2 B_* + (\nu + 1)s^2 B_2, \quad (\text{Appendix C.5b})$$

363 where no superscript appears at LHS in light of (25). This system of equations provides a non-singular
 364 constant-coefficient linear transformation of the functions B_* and B_2 to \bar{m}_0 and \bar{v}_0 , whence these share the
 365 same asymptotics. We may easily solve the linear system

$$\begin{bmatrix} B_* \\ B_2 \end{bmatrix} = \begin{bmatrix} 1 - \nu & 2 \\ \nu - 1 & 1 + \nu \end{bmatrix}^{-1} \begin{bmatrix} \beta^{-1} \bar{m}_0 \\ s^{-2} \bar{v}_0 \end{bmatrix} = \frac{1}{4c} \begin{bmatrix} 1 + \nu & -2 \\ 1 - \nu & 1 - \nu \end{bmatrix} \begin{bmatrix} \beta^{-1} \bar{m}_0 \\ s^{-2} \bar{v}_0 \end{bmatrix}, \quad (\text{Appendix C.6})$$

366 to get

$$B_* = \frac{(1 + \nu)\bar{m}_0\beta^{-1} - 2\bar{v}_0s^{-2}}{(1 - \nu)(3 + \nu)}, \quad B_2 = \frac{1}{3 + \nu} (\bar{m}_0\beta^{-1} + \bar{v}_0s^{-2}). \quad (\text{Appendix C.7})$$

367 *Appendix C.1.3. Refined asymptotics at zero*

368 Taking advantage of the results (35), we can better determine the asymptotics of B_* and B_2 (and likewise
 369 for A_1, A_2) as $s \rightarrow 0$. We begin with the transformed bending moment $\bar{m}_0(s)$. First, it follows from (21) and
 370 (16b), that $m_0^{A,B}(x_1) \in L_1(\mathbb{R})$, $x_1 m_0^{A,B}(x_1) \in L_1(\mathbb{R})$, as a result, we conclude that $\bar{m}_0(s) = \bar{m}(s, 0) \in \mathbb{C}_{loc}^1$
 371 and thus

$$\bar{m}_0(s) = \mathbf{m}_0 + \mathbf{m}_1 s + O(|s|^{3/2}), \quad s \rightarrow 0. \quad (\text{Appendix C.8})$$

372 Similarly, it follows from (21) and (16c), that $v_0^{A,B}(x_1) \in L_1(\mathbb{R})$, $x_1 v^{A,B}(x_1) \in L_1(\mathbb{R})$ and $x_1^2 v^{A,B}(x_1) \in$
 373 $L_1(\mathbb{R})$, as a result, we conclude that $\bar{v}_0(s) = \bar{v}(s, 0) \in \mathbb{C}_{loc}^2$ near the origin and thus

$$\bar{v}_0(s) = \mathbf{v}_0 + \mathbf{v}_1 s + \mathbf{v}_2 s^2 + O(|s|^{5/2}), \quad s \rightarrow 0. \quad (\text{Appendix C.9})$$

374 From the transformed balance conditions (27), it immediately follows that $\mathbf{m}_0 = \mathbf{v}_0 = \mathbf{v}_1 = 0$. Besides,
 375 plugging (Appendix C.4, Appendix C.7) into (35a), one gets

$$\llbracket \bar{w} \rrbracket \sim a_1 s^{\varpi_1} + a_2 s^{\varpi_2} - \frac{1}{(1-\nu)(3+\nu)} \left((1+\nu) \mathbf{m}_1 \text{sign } s - 2\mathbf{v}_2 \right) \beta^{-1} + O(|s|^{-1/2}), \quad s \rightarrow 0, \quad (\text{Appendix C.10})$$

and for this to be consistent with the first of (20) it is necessary that the β^{-1} -term drops out, i.e. $\pm(1+\nu)\mathbf{m}_1 =$
 $2\mathbf{v}_2$ as $s \rightarrow \pm 0$. Similarly, using (Appendix C.4, Appendix C.7) into (35b) and recalling (30), we get

$$\begin{aligned} \llbracket \bar{\phi} \rrbracket \sim & -e^{-i\pi/4} a_1 s^{\varpi_1} - e^{i\pi/4} a_2 s^{\varpi_2} - \frac{1}{(1-\nu)(3+\nu)} \left((1+\nu) \mathbf{m}_1 \text{sign } s - 2\mathbf{v}_2 \right) \\ & - \frac{1}{3+\nu} \left(\mathbf{m}_1 \text{sign } s + \mathbf{v}_2 \right) + O(|s|^{1/2}), \quad s \rightarrow 0, \quad (\text{Appendix C.11}) \end{aligned}$$

376 and the constant term needs to disappear, i.e. $\pm\mathbf{m}_1 = \mathbf{v}_2$ as $s \rightarrow \pm 0$. As a result, one concludes that

$$\mathbf{m}_1 = \mathbf{v}_2 = 0. \quad (\text{Appendix C.12})$$

377 Then, we can write the respective assumptions for $\bar{m}_0(s)$ and $\bar{v}_0(s)$ more accurately

$$\bar{m}_0(s) = O(|s|^{3/2}), \quad \bar{v}_0(s) = O(|s|^{5/2}), \quad s \rightarrow 0, \quad (\text{Appendix C.13})$$

378 and returning back to (Appendix C.7) we conclude that

$$B_*(s), B_2(s) = O(|s|^{1/2}), \quad s \rightarrow 0. \quad (\text{Appendix C.14})$$

379 With this knowledge, returning back to Eq.(35c) while substituting the asymptotics (Appendix C.4, Appendix
 380 C.14), we get

$$\bar{m}_0^A = -i a_1 s^{\varpi_1} + i a_2 s^{\varpi_2} = O(|s|^{3/2}), \quad s \rightarrow 0. \quad (\text{Appendix C.15})$$

381 The same argument, this time applied to (35d), gives

$$\bar{v}_0^A = -e^{-i3\pi/4} a_1 s^{\varpi_1} - e^{i3\pi/4} a_2 s^{\varpi_2} = O(|s|^{5/2}), \quad s \rightarrow 0, \quad (\text{Appendix C.16})$$

382 and the system (Appendix C.15, Appendix C.16) is consistent only if

$$\varpi_1 = \varpi_2 = \frac{3}{2}, \quad (\text{Appendix C.17})$$

383 and we finally prove that the asymptotics (Appendix C.3) is incorrect. Furthermore, plugging this result
 384 into (Appendix C.16), one sees that

$$a_1 = i a_2, \quad (\text{Appendix C.18})$$

385 whence we obtain the leading asymptotics of \bar{w}_0^A and $\bar{\phi}_0^A$ at the origin, namely

$$\bar{w}_0^A = A_1 + A_2 = (1+i)a_2 s^{3/2}, \quad \bar{\phi}_0^A = -\alpha_1 A_1 - \alpha_2 A_2 = -\sqrt{2}(1+i)a_2 s^{3/2}, \quad s \rightarrow 0. \quad (\text{Appendix C.19})$$

386 *Appendix C.2. Asymptotic behavior at $s \rightarrow \pm\infty$*

387 From the Abelian theorem [22] applied to (16b), it follows

$$\bar{m}_0^+(s) = \mathbf{m}_\infty e^{\pm i\pi/4} |s|^{-1/2} + O(|s|^{-1}), \quad s \rightarrow \pm\infty, \quad (\text{Appendix C.20})$$

where, clearly,

$$\mathbf{m}_\infty = \frac{12\sqrt{\pi}c}{\nu+7} \mathcal{K}_e.$$

388 Likewise, from (10), it is

$$\bar{m}_0^-(s) \equiv \bar{M}_0^-(s) = O(s^{-1-\gamma_0}), \quad |s| \rightarrow \infty, \quad \Im(s) < 0, \quad (\text{Appendix C.21})$$

389 that, recalling $\gamma_0 > \frac{1}{2}$, decays faster than (Appendix C.20). Thus, summing (Appendix C.20) and (Appendix C.21)
390 together, we have

$$\bar{m}_0(s) = b_1 |s|^{-1/2} = \mathbf{m}_\infty e^{\pm i\pi/4} |s|^{-1/2} + O(|s|^{-1}), \quad s \rightarrow \pm\infty. \quad (\text{Appendix C.22})$$

391 In similar fashion, it follows from (16c) and the Abelian theorem that

$$\bar{v}_0^+(s) = \mathbf{v}_\infty e^{\mp i\pi/4} |s|^{1/2} + O(1), \quad s \rightarrow \pm\infty, \quad (\text{Appendix C.23})$$

with

$$\mathbf{v}_\infty = \frac{12\sqrt{\pi}c}{3\nu+5} \mathcal{K}_o.$$

392 Again, the applied shearing force decays faster because it was assumed $\gamma_0 > \frac{1}{2}$

$$\bar{v}_0^-(s) = \bar{V}_0^-(s) = O(s^{-\gamma_0}), \quad |s| \rightarrow \infty, \quad \Im(s) < 0, \quad (\text{Appendix C.24})$$

393 whence, summing, one gets

$$\bar{v}_0(s) = b_2 |s|^{\frac{1}{2}} = \mathbf{v}_\infty e^{\mp i\pi/4} |s|^{\frac{1}{2}} + O(1), \quad s \rightarrow \pm\infty, \quad (\text{Appendix C.25})$$

394 whose diverging character denotes that this is a Fourier transform in the sense of distributions.

395 Substituting the asymptotics (Appendix C.22) and (Appendix C.25) into (33b) and (33c), respectively,
396 we get a linear system for the asymptotics of $A_{1,2}(s)$, namely

$$\begin{cases} (\alpha_1^2 - \nu s^2)A_1 + (\alpha_2^2 - \nu s^2)A_2 = b_1 |s|^{-1/2}, \\ -\alpha_1(\alpha_1^2 + (\nu - 2)s^2)A_1 - \alpha_2(\alpha_2^2 + (\nu - 2)s^2)A_2 = b_2 |s|^{1/2}, \end{cases} \quad s \rightarrow \pm\infty. \quad (\text{Appendix C.26})$$

397 Lets write this system in the form

$$\mathbf{M}\mathbf{a} = \mathbf{b}, \quad s \rightarrow \pm\infty, \quad (\text{Appendix C.27})$$

398 where

$$\mathbf{M} = \begin{bmatrix} \alpha_1^2 - \nu s^2 & \alpha_2^2 - \nu s^2 \\ -\alpha_1(\alpha_1^2 + (\nu - 2)s^2) & -\alpha_2(\alpha_2^2 + (\nu - 2)s^2) \end{bmatrix}, \quad (\text{Appendix C.28})$$

399 and

$$\mathbf{b} \sim [b_1 |s|^{-1/2}, b_2 |s|^{1/2}], \quad s \rightarrow \pm\infty, \quad (\text{Appendix C.29})$$

400 This system is nonsingular (at least at infinity), for we have

$$\det \mathbf{M} = -4ic |s|^3 + O(|s|^{-1}), \quad s \rightarrow \pm\infty. \quad (\text{Appendix C.30})$$

401 Hence, it can be solved giving

$$\begin{cases} A_1 = \frac{i(b_1 - b_2)}{\nu + 3} |s|^{-1/2} + \frac{b_1(\nu + 1) + 2b_2}{2(1 - \nu)(\nu + 3)} |s|^{-5/2} + o(|s|^{-5/2}), \\ A_2 = -\frac{i(b_1 - b_2)}{\nu + 3} |s|^{-1/2} + \frac{b_1(\nu + 1) + 2b_2}{2(1 - \nu)(\nu + 3)} |s|^{-5/2} + o(|s|^{-5/2}), \end{cases} \quad s \rightarrow \pm\infty. \quad (\text{Appendix C.31})$$

By substituting this expansion into the general solution (29) for the supported plate, we obtain, to leading order,

$$\bar{w}_0^A = A_1 + A_2 = \frac{b_1(\nu + 1) + 2b_2}{(1 - \nu)(\nu + 3)} |s|^{-5/2}, \quad s \rightarrow \pm\infty,$$

402 whence

$$\bar{w}_0^A = 3\sqrt{\pi} \left(e^{\pm i\pi/4} \mathcal{K}_e \frac{\nu + 1}{\nu + 7} + e^{\mp i\pi/4} \mathcal{K}_o \frac{2}{3\nu + 5} \right) |s|^{-5/2}, \quad s \rightarrow \pm\infty. \quad (\text{Appendix C.32})$$

Similarly, substituting (Appendix C.31) into (33a), we get

$$\bar{\phi}_0^A = -\alpha_1 A_1 - \alpha_2 A_2 = -\frac{b_2(\nu + 1) + 2b_1}{(1 - \nu)(\nu + 3)} |s|^{-3/2},$$

403 thus, to leading order,

$$\bar{\phi}_0^A = -3\sqrt{\pi} e^{\pm i\pi/4} \left(\frac{2}{\nu + 7} \mathcal{K}_e \pm i \frac{\nu + 1}{3\nu + 5} \mathcal{K}_o \right) |s|^{-3/2}, \quad s \rightarrow \pm\infty. \quad (\text{Appendix C.33})$$

404 *Appendix C.3. Asymptotics of the half-transforms \bar{w}^\pm , $\bar{\phi}^\pm$, \bar{m}^\pm , \bar{v}^\pm*

In the previous Sections, we have obtained the asymptotics of the full range Fourier transforms, both as $s \rightarrow 0$ and as $s \rightarrow \pm\infty$, see Table C.2. Moving from these, we here deduce, the corresponding behaviour of

| | $s \rightarrow 0$ | $ s \rightarrow \infty$ |
|---|-------------------|--------------------------|
| \bar{w}_0^A | $s^{3/2}$ | $s^{-5/2}$ |
| $\bar{\phi}_0^A$ | $s^{3/2}$ | $s^{-3/2}$ |
| $\bar{m}_0 = \bar{m}^+$ | $s^{3/2}$ | $s^{-1/2}$ |
| $\bar{v}_0 = \bar{v}^+$ | $s^{5/2}$ | $s^{1/2}$ |
| $\llbracket \bar{w} \rrbracket = \llbracket \bar{w}^- \rrbracket$ | $s^{-1/2}$ | $s^{-5/2}$ |
| $\llbracket \bar{\phi} \rrbracket = \llbracket \bar{\phi}^- \rrbracket$ | $s^{1/2}$ | $s^{-3/2}$ |

Table C.2: Asymptotics of the full range Fourier transforms

the half-transforms. From the Taylor expansion of (23) as $s \rightarrow 0$, we write

$$\bar{\phi}_0^+(s) = \int_0^\infty \phi_0(x) dx + O(s^{1/2}), \quad \bar{\phi}_0^B(s) = \int_{-\infty}^0 \phi_0^B(x) dx + O(s^{1/2}), \quad s \rightarrow 0, \quad (\text{Appendix C.34a})$$

$$\bar{m}_0^+(s) = \int_0^{+\infty} m_0(x) dx + is \int_0^{+\infty} x m_0(x) dx + O(s^{3/2}), \quad s \rightarrow 0, \quad (\text{Appendix C.34b})$$

$$\bar{m}_0^-(s) = \int_{-\infty}^0 M_0(x) dx + is \int_{-\infty}^0 x M_0(x) dx + O(s^2), \quad s \rightarrow 0, \quad (\text{Appendix C.34c})$$

$$\bar{v}_0^+(s) = \int_0^{+\infty} v_0(x) dx + is \int_0^{+\infty} x v_0(x) dx - \frac{1}{2} s^2 \int_0^{+\infty} x^2 v_0(x) dx + O(s^{5/2}), \quad s \rightarrow 0, \quad (\text{Appendix C.34d})$$

$$\bar{v}_0^-(s) = \int_{-\infty}^0 V_0(x) dx + is \int_{-\infty}^0 x V_0(x) dx - \frac{1}{2} s^2 \int_{-\infty}^0 x^2 V_0(x) dx + O(s^3), \quad s \rightarrow 0. \quad (\text{Appendix C.34e})$$

Accounting for (Appendix C.13), we deduce the asymptotics

$$\bar{m}_0^+(s) = -\bar{M}_0^-(0) - s \frac{d\bar{M}_0^-}{ds}(0) + O(s^{3/2}), \quad s \rightarrow 0, \quad (\text{Appendix C.35a})$$

$$\bar{v}_0^+(s) = -\bar{V}_0^-(0) - s \frac{d\bar{V}_0^-}{ds}(0) - \frac{1}{2} s^2 \frac{d^2 \bar{V}_0^-}{ds^2}(0) + O(s^{5/2}), \quad s \rightarrow 0. \quad (\text{Appendix C.35b})$$

405 Also, from (Appendix C.10) and (Appendix C.11) we have

$$[[\bar{w}]] = O(s^{-1/2}), \quad [[\bar{\phi}]] = \bar{\phi}_0^A - (\bar{\phi}_0^+ + \bar{\phi}_0^{B-}) = O(s^{1/2}), \quad s \rightarrow 0, \quad (\text{Appendix C.36})$$

where, recalling (Appendix C.19), it is $\bar{w}_0^A = O(s^{3/2})$ and $\bar{\phi}_0^A = O(s^{3/2})$. For the last asymptotics to hold true, it is required that

$$\int_{-\infty}^{\infty} \phi_0(s) dx = 0.$$

The asymptotics at infinity are compute directly taking the positive half-transform of (14,16)

$$\bar{w}_0^+(s) = iW_0s^{-1} - W_1s^{-2} + 3\sqrt{\pi}\frac{\nu+1}{\nu+7}e^{\pm i\pi/4}\mathcal{K}_e|s|^{-5/2} + O(s^{-7/2}), \quad s \rightarrow \pm\infty, \quad (\text{Appendix C.37a})$$

$$\bar{\phi}_0^+(s) = iW_2s^{-1} - 3\sqrt{\pi}\frac{\nu+1}{3\nu+5}e^{\mp i\pi/4}\mathcal{K}_o|s|^{-3/2} + O(s^{-5/2}), \quad s \rightarrow \pm\infty, \quad (\text{Appendix C.37b})$$

$$\bar{m}_0^+(s) = 12c\sqrt{\pi}\frac{e^{\pm i\pi/4}}{\nu+7}\mathcal{K}_e|s|^{-1/2} + O(s^{-3/2}), \quad s \rightarrow \pm\infty, \quad (\text{Appendix C.37c})$$

$$\bar{v}_0^+(s) = 12c\sqrt{\pi}\frac{e^{\mp i\pi/4}}{3\nu+5}\mathcal{K}_o|s|^{1/2} + C_1 + O(s^{-1/2}), \quad s \rightarrow \pm\infty. \quad (\text{Appendix C.37d})$$

where the first two formulae are valid inasmuch as $\Im(s) > 0$ and the last only in the sense of distributions. Similarly, for the negative half transforms, we get

$$\bar{w}_0^{B-}(s) = -iW_0s^{-1} + W_1s^{-2} - 6\sqrt{\pi}\frac{e^{\mp i\pi/4}}{3\nu+5}\mathcal{K}_o|s|^{-5/2} + O(|s|^{-7/2}), \quad s \rightarrow \pm\infty, \quad (\text{Appendix C.38a})$$

$$\bar{\phi}_0^{B-}(s) = -iW_2s^{-1} + 6\sqrt{\pi}\frac{e^{\pm i\pi/4}}{\nu+7}\mathcal{K}_e|s|^{-3/2} + O(s^{-5/2}), \quad s \rightarrow \pm\infty, \quad (\text{Appendix C.38b})$$

$$\bar{m}_0^-(s) = \bar{M}_0^-(s) = O(s^{-\gamma_0-1}), \quad \bar{v}_0^-(s) = \bar{V}_0^-(s) = O(s^{-\gamma_0}), \quad s \rightarrow \infty, \quad (\text{Appendix C.38c})$$

406 Accounting for (Appendix C.32, Appendix C.33), we obtain, to leading order,

$$\begin{aligned} [[\bar{w}]] &= \bar{w}_0^A - (\bar{w}_0^+ + \bar{w}^{B-}) \sim 12\sqrt{\pi}\frac{e^{\mp i\pi/4}}{5+3\nu}\mathcal{K}_o|s|^{-5/2}, \\ [[\bar{\phi}]] &= \bar{\phi}_0^A - (\bar{\phi}_0^+ + \bar{\phi}^{B-}) \sim -12\sqrt{\pi}\frac{e^{\pm i\pi/4}}{7+\nu}\mathcal{K}_e|s|^{-3/2}, \quad s \rightarrow \pm\infty. \\ \bar{m}_0 &\sim \mathbf{m}_\infty e^{\pm i\pi/4}\mathcal{K}_e|s|^{-1/2}, \quad \bar{v}_0 \sim \mathbf{v}_\infty e^{\mp i\pi/4}\mathcal{K}_o|s|^{1/2}, \end{aligned} \quad (\text{Appendix C.39})$$

407 References

- 408 [1] DD Ang, ES Folias, and ML Williams. The bending stress in a cracked plate on an elastic foundation.
409 *Journal of Applied Mechanics*, 1963.
- 410 [2] T Atkins. *The science and engineering of cutting: the mechanics and processes of separating, scratching*
411 *and puncturing biomaterials, metals and non-metals*. Butterworth-Heinemann, 2009.
- 412 [3] Z-Q Cheng and JN Reddy. Green's functions for an anisotropic thin plate with a crack or an anticrack.
413 *International journal of engineering science*, 42(3-4):271–289, 2004.
- 414 [4] K-R Deibel, C Raemy, and K Wegener. Modeling slice-push cutting forces of a sheet stack based on
415 fracture mechanics. *Engineering Fracture Mechanics*, 124:234–247, 2014.
- 416 [5] ES Folias. On a plate supported by an elastic foundation and containing a finite crack. *International*
417 *Journal of Fracture Mechanics*, 6(3):257–263, 1970.
- 418 [6] J P Gallagher. Usaf damage tolerant design handbook: guidelines for the analysis and design of damage
419 tolerant aircraft structures. Technical report, 1984.

- 420 [7] R V Gol'dstein and R L Salganik. Brittle fracture of solids with arbitrary cracks. *International journal*
421 *of Fracture*, 10:507–523, 1974.
- 422 [8] N Gorbushin, V Eremeyev, and G Mishuris. On stress singularity near the tip of a crack with surface
423 stresses. *International Journal of Engineering Science*, 146:103183, 2020.
- 424 [9] RJ Hartranft and GC Sih. An approximate three-dimensional theory of plates with application to crack
425 problems. *International Journal of Engineering Science*, 8(8):711–729, 1970.
- 426 [10] C-W Hsu and C Hwu. Green's functions for unsymmetric composite laminates with inclusions. *Pro-*
427 *ceedings of the Royal Society A*, 476(2233):20190437, 2020.
- 428 [11] Zhen-Liang Hu, Xue-Yang Zhang, and Xian-Fang Li. Oscillatory singularity for bending of a partially
429 clamped nanoplate with consideration of surface effect. *Engineering Fracture Mechanics*, page 109495,
430 2023.
- 431 [12] I.S.Gradshteyn and I.M.Ryzhik. *Tables of integrals, series and products*. Academic Press, fifth edition,
432 1996.
- 433 [13] VGMD Kumar, MD German, and C F Shih. Engineering approach for elastic-plastic fracture analysis.
434 Technical report, General Electric Co., 1981.
- 435 [14] H Liebowitz and GC Sih. Mathematical theories of brittle fracture. chapter 2. ACADEMIC PRESS,
436 INC., 1968.
- 437 [15] P C Miedlar, A P Berens, A Gunderson, and JP Gallagher. Analysis and support initiative for structural
438 technology (asist) delivery order 0016: Usaf damage tolerant design handbook: guidelines for the analysis
439 and design of damage tolerant aircraft structures. Technical report, DAYTON UNIV OH RESEARCH
440 INST, 2002.
- 441 [16] SA Mohamed, S Bichir, MS Matbuly, and M Nassar. Analytical solution of cracked shell resting on
442 elastic foundation. *Acta mechanica solida sinica*, 9(4):306–319, 1996.
- 443 [17] A Nobili, E Radi, and L Lanzoni. A cracked infinite kirchhoff plate supported by a two-parameter
444 elastic foundation. *Journal of the European Ceramic Society*, 34(11):2737–2744, 2014.
- 445 [18] A Nobili, E Radi, and L Lanzoni. On the effect of the backup plate stiffness on the brittle failure of a
446 ceramic armor. *Acta Mechanica*, 227:159–172, 2016.
- 447 [19] A Nobili, E Radi, and L Lanzoni. Flexural edge waves generated by steady-state propagation of a
448 loaded rectilinear crack in an elastically supported thin plate. *Proceedings of the Royal Society A:*
449 *Mathematical, Physical and Engineering Sciences*, 473(2204):20170265, 2017.
- 450 [20] Andrea Nobili and Valentina Volpini. Microstructured induced band pattern in love wave propagation for
451 novel nondestructive testing (ndt) procedures. *International Journal of Engineering Science*, 168:103545,
452 2021.
- 453 [21] B Noble. *Methods based on the Wiener-Hopf technique for the solution of partial differential equations*,
454 *International Series of Monographs on Pure and Applied Mathematics. Vol. 7*. Pergamon Press, New
455 York, 1958.
- 456 [22] A Piccolroaz, G Mishuris, and A Movchan. Symmetric and skew-symmetric weight functions in 2d
457 perturbation models for semi-infinite interfacial cracks. *Journal of the Mechanics and Physics of Solids*,
458 57:1657–1682, 2009.
- 459 [23] A Piccolroaz, D Peck, M Wrobel, and G Mishuris. Energy release rate, the crack closure integral
460 and admissible singular fields in fracture mechanics. *International Journal of Engineering Science*,
461 164:103487, 2021.

- 462 [24] Y Pronina, A Maksimov, and M Kachanov. Crack approaching a domain having the same elastic
463 properties but different fracture toughness: Crack deflection vs penetration. *International Journal of*
464 *Engineering Science*, 156:103374, 2020.
- 465 [25] DV Ramsamooj. Fracture of highway and airport pavements. *Engineering Fracture Mechanics*,
466 44(4):609–626, 1993.
- 467 [26] S Rogosin and G Mishuris. Constructive methods for factorization of matrix-functions. *IMA Journal*
468 *of Applied Mathematics*, 81:365–391, 2016.
- 469 [27] G C Sih. Bending of a cracked plate with arbitrary stress distribution across the thickness. Technical
470 report, NASA Technical report Nr.6, 1969.
- 471 [28] G C Sih. A review of the three-dimensional stress problem for a cracked plate. *International Journal*
472 *of Fracture Mechanics*, 7(1):39–61, 1971.
- 473 [29] G C Sih. *Plates and shells with cracks: a collection of stress intensity factor solutions for cracks in*
474 *plates and shells*, volume 3. Springer Science & Business Media, 2012.
- 475 [30] L Slepyan. Forced waves in a uniform waveguide with distributed and localized dynamic structures
476 attached. *International Journal of Engineering Science*, 173:103628, 2022.
- 477 [31] M L Williams. The bending stress distribution at the base of a stationary crack. *J. Appl. Mech.*, pages
478 78–82, 1961.
- 479 [32] Haiying Zhang, Zhenwen Zhou, Alexander Chudnovsky, and Hoang Pham. Time-dependent buckling
480 delamination of thin plastic films and their conformability: Observations and modeling. *International*
481 *Journal of Engineering Science*, 150:103258, 2020.
- 482 [33] Z. Zhuang, Z. Liu, B. Cheng, and J. Liao. *Extended finite element method*, chapter X-FEM on
483 Continuum-Based Shell Elements. Tsinghua University Press computational mechanics series. Tsinghua
484 University Press, Beijing, 2014.

Declaration of interests

The authors declare that they have no known competing financial interests or personal relationships that could have appeared to influence the work reported in this paper.

The authors declare the following financial interests/personal relationships which may be considered as potential competing interests:

Andrea Nobili reports financial support was provided by Government of Italy Ministry of Education University and Research. Gennady Mishuris reports a relationship with European Union that includes: funding grants.